

Statistical Physics of Synchronized Traffic Flow: Spatiotemporal Competition between S→F and S→J Instabilities

Boris S. Kerner¹

¹ *Physics of Transport and Traffic, University Duisburg-Essen, 47048 Duisburg, Germany*

We have revealed statistical physics of synchronized traffic flow that is governed by a spatiotemporal competition between S→F and S→J instabilities (where F, S, and J denote, respectively, the free flow, synchronized flow, and wide moving jam traffic phases). A probabilistic analysis of synchronized flow based on simulations of a cellular automaton model in the framework of three-phase traffic theory is made. This probabilistic analysis shows that there is a finite range of the initial space-gap between vehicles in synchronized flow within which during a chosen time for traffic observation either synchronized flow persists with probability P_S , or an S→F transition occurs with probability P_{SF} , or else an S→J transition occurs with probability P_{SJ} . Space-gap dependencies of the probabilities P_S , P_{SF} , and P_{SJ} have been found. It has been also found that (i) an initial S→F instability can lead to sequences of S→F→S→J transitions; (ii) an initial S→J instability can lead to sequences of S→J→S→F transitions. Each of the phase transitions in the sequences S→F→S→J transitions and S→J→S→F transitions exhibits the nucleation nature; these sequences of phase transitions determine spatiotemporal features of traffic patterns resulting from the competition between S→F and S→J instabilities. The statistical features of synchronized flow found for a homogeneous road remain qualitatively for a road with a bottleneck. However, rather than nuclei for S→F and S→J instabilities occur at random road locations of the homogeneous road, due to a permanent non-homogeneity introduced by the bottleneck, nuclei for initial S→F and S→J instabilities appear mostly at the bottleneck.

PACS numbers: 89.40.-a, 47.54.-r, 64.60.Cn, 05.65.+b

I. INTRODUCTION

Vehicle traffic occurs in space and time. Empirical traffic data measured in space and time shows that well-known empirical moving jams [1–3] occur in free flow through a sequence of F→S→J phase transitions of three-phase traffic theory (three-phase theory for short) (F – free flow, S – synchronized flow, J – wide moving jam) [4, 5]: Firstly, traffic breakdown in free flow at a bottleneck occurs that is a phase transition from free flow to synchronized flow (F→S transition). Later and usually at a different road location a phase transition from synchronized flow to a wide moving jam (J) can be realized (S→J transition). A typical empirical example of a such sequence of F→S→J transitions is shown in Fig. 1 (a, b). Features of empirical F→S and S→J transitions between the three traffic phases F, S, and J (Fig. 1 (b)) have been explained in the three-phase theory [4] by the existence two qualitatively different instabilities in the synchronized flow traffic phase: S→F instability and S→J instability (Fig. 1 (c, d)) [6–8].

The main reason of the three-phase theory is the explanation of the empirical nucleation nature of traffic breakdown (F→S transition) at the bottleneck. To reach this goal, in congested traffic a new traffic phase called synchronized flow has been introduced [4, 5]. The basic feature of the synchronized flow traffic phase formulated in the three-phase theory leads to the nucleation nature of the F→S transition. In this sense, the synchronized flow traffic phase, which ensures the nucleation nature of the F→S transition at a highway bottleneck, and the three-phase traffic theory can be considered synonymous.

An S→J instability is a growing wave of a local *speed decrease* in synchronized flow. As shown in [6], the S→J instability is associated with the classical traffic flow instability introduced and developed in 1958–1961 by Herman, Gazis, Montroll, Potts, Rothery, and Chandler [10–13] from General Motors (GM) Company. The classical traffic flow instability is associated with a driver over-deceleration effect: If a vehicle begins to decelerate unexpectedly, then due to a finite driver reaction time the following vehicle starts deceleration with a delay. As a result, the speed of the following vehicle becomes lower than the speed of the preceding vehicle. If this over-deceleration effect is realized for following drivers, the traffic flow instability occurs. With the use of very different mathematical approaches, the classical traffic flow instability has been incorporated in a huge number of traffic flow models (see, e.g., [14–31] and reviews [32–34]). All these different traffic flow models can be considered belonging to the same GM model class. Indeed, as found firstly in 1993–1994 [35], in all these very different traffic flow models the classical instability leads to a moving jam (J) formation in free flow (F) (F→J transition) (see references in [6–8, 33, 34]). The classical instability of the GM model class should explain traffic breakdown, i.e., a transition from free flow to congested traffic observed in real traffic [10–33]). However, as shown in [6–8, 34], traffic flow models of the GM model class (see references in [6–8, 34]) failed in the explanation of real traffic breakdown. This is because rather than an F→J transition of the models of the GM model class, in all real field traffic data traffic breakdown is an F→S transition occurring in metastable free flow with respect to

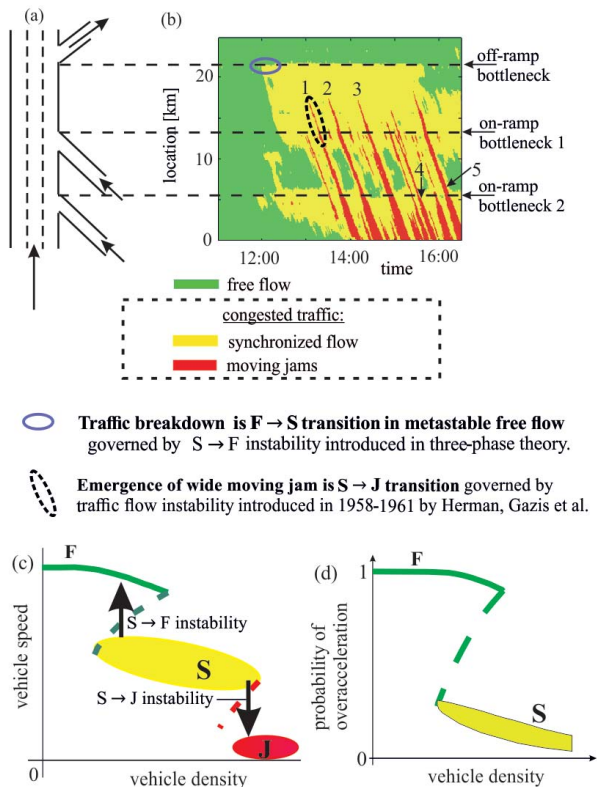


FIG. 1: Explanation of two traffic flow instabilities of three-phase theory [6–8]: (a, b) Typical empirical example of a fragment of complex congested traffic pattern measured on a highway section with three highway bottlenecks (highway A5-North in Germany) on March 23, 2001; (a) sketch of highway section (off-ramp bottleneck and two on-ramp bottlenecks); (b) empirical speed data presented in space and time with averaging method described in Sec. C.2 of [9]. (c) Hypothesis of three-phase theory about phase transitions in traffic flow: 2Z-characteristic for phase transitions [6, 38]. (d) Hypothesis of three-phase theory about discontinuous character of over-acceleration probability [5–7, 38, 39]. F – free flow phase, S – synchronized flow phase, J – wide moving jam phase.

the $F \rightarrow S$ transition [4–8, 34, 36–42].

In contrast with the $S \rightarrow J$ instability that is a growing wave of a local *speed reduction* in synchronized flow, an $S \rightarrow F$ instability is a growing wave of a local *speed increase* in synchronized flow. As shown in [43], the $S \rightarrow F$ instability exhibits the nucleation nature. The nucleation nature of the $S \rightarrow F$ instability governs the nucleation nature of the $F \rightarrow S$ transition at the bottleneck. The $S \rightarrow F$ instability is associated with the over-acceleration effect [5–8, 34, 38, 39]. It is assumed that probability of over-acceleration should exhibit a discontinuous character (Fig. 1 (d)) that is associated with a driver time-delay in over-acceleration [6–8, 34, 38, 39].

The first mathematical implementation of hypotheses

of the three-phase theory [4–7, 37–39] has been a stochastic continuous in space microscopic model [44] and a cellular automaton (CA) three-phase model [45], which have been further developed for different applications in [46–61]. Over time there has been developed a number of other traffic flow models (e.g., [62–113]) that incorporate some of the hypotheses of the three-phase theory [5–7, 38, 39].

Separately from each other the $S \rightarrow F$ and $S \rightarrow J$ instabilities have already been studied (for a review see, e.g., [8, 48]). However, from the hypotheses of the three-phase theory it could be expected that there should be a competition between the $S \rightarrow J$ and $S \rightarrow F$ instabilities in synchronized traffic flow. Such a competition between the two qualitatively different traffic flow instabilities in synchronized flow has *not* been found up to now.

In this paper, we have revealed that there is indeed a spatiotemporal competition between the $S \rightarrow J$ and $S \rightarrow F$ instabilities. It has been found that this competition effects considerably on statistical features of vehicular traffic flow. Either the $S \rightarrow J$ instability [6] or the $S \rightarrow F$ instability exhibits the nucleation nature [43]. For this reason, to study probabilistic features of the *spontaneous* occurrence of these instabilities as well as their competition, we use a stochastic traffic flow model with a relatively large amplitude of model fluctuations. This model feature exhibits the KKSJ (Kerner-Klenov-Schreckenberg-Wolf) CA (cellular automaton) three-phase traffic flow model [45, 56, 57]. Because the KKSJ CA model has already been published, we present it in Appendix A. Main contributions of this paper are as follows:

(i) We show that there is a finite range of the initial space-gap between vehicles in synchronized flow within which during a chosen time T_{ob} for traffic observation either synchronized flow persists with probability P_S , or firstly an $S \rightarrow F$ transition occurs in synchronized flow with probability P_{SF} , or else firstly an $S \rightarrow J$ transition occurs in synchronized flow with probability P_{SJ} .

(ii) It has been also found that an $S \rightarrow F$ transition can lead to sequences of $S \rightarrow F \rightarrow S \rightarrow J$ transitions.

(iii) We show that an $S \rightarrow J$ transition can lead to sequences of $S \rightarrow J \rightarrow S \rightarrow F$ transitions.

(iv) The sequences of phase transitions of items (ii) and (iii) determine spatiotemporal features of traffic patterns resulting from the competition between $S \rightarrow F$ and $S \rightarrow J$ instabilities.

(v) The above statistical features of vehicular traffic found for a homogeneous road remain qualitatively for a road with an on-ramp bottleneck. In particular, flow-rate dependencies of the probabilities P_S , P_{SF} , and P_{SJ} for synchronized flow at the bottleneck are qualitatively the same as the space-gap dependencies of these probabilities found in the paper for the homogeneous road. The main difference between the latter two cases is that due to a permanent non-homogeneity introduced by a bottleneck, nuclei for initial $S \rightarrow F$ and $S \rightarrow J$ instabilities appear mostly at the bottleneck.

The article is organized as follows. In Sec. II, we de-

velop the statistical physics of the $S \rightarrow F$ and $S \rightarrow J$ transitions occurring due to the spatiotemporal competition of $S \rightarrow F$ and $S \rightarrow J$ instabilities in the same initial state of synchronized flow on a homogeneous road. In particular, we study probabilistic characteristics of the phase transitions and microscopic effects governing the phase transitions. In Sec. III, these results of the statistical physics of synchronized flow are applied for a study of traffic phenomena occurring in synchronized flow at an on-ramp bottleneck. In Discussion, we consider the effect of the average space gap between vehicles on congested patterns (Sec. IV A), the evolution of congested patterns at a bottleneck due to the change in the on-ramp inflow rate (Sec. IV B), some peculiarities of synchronized flow that occurs spontaneously at the bottleneck after sequences of $F \rightarrow S \rightarrow F$ transitions (Sec. IV C) as well as formulate conclusions of the paper.

II. PROBABILISTIC FEATURES OF COMPETITION BETWEEN $S \rightarrow F$ AND $S \rightarrow J$ INSTABILITIES ON CIRCULAR HOMOGENEOUS ROAD

To reveal statistical features of synchronized flow governed by the competition between $S \rightarrow F$ and $S \rightarrow J$ instabilities, in Sec. II we have simulated a spatiotemporal evolution of synchronized flow on a circular homogeneous single-lane road (road length is 25 km) (Fig. 2). We have made a large number N_r (where $N_r \gg 1$) of different simulation realizations (runs) in which a diverse variety of critical traffic spatiotemporal phenomena occur with different probabilities. Some characteristic realizations are presented in Figs. 2 (a–g). In each of the realizations the initial state of synchronized flow on the whole road is a spatially homogeneous one and it is the same [115]: At time instant $t = 0$, all vehicles are located at the same chosen initial space gap between vehicles g_{ini} ; all vehicles begin to move simultaneously at the same initial chosen synchronized flow speed $v_{ini}^{(syn)}$.

A. A diverse variety of critical phenomena found in different realizations simulated at the same model parameters

It turns out that the existence of the diverse variety of critical traffic phenomena (Fig. 2) is indeed associated with a spatiotemporal competition between $S \rightarrow F$ and $S \rightarrow J$ instabilities in synchronized flow. We have found three *basic* cases of this spatiotemporal competition:

- (i) Neither the $S \rightarrow F$ instability nor the $S \rightarrow J$ instability that emerge randomly on different road locations leads to $S \rightarrow F$ or $S \rightarrow J$ transitions. This is because the development of each of the instabilities is interrupted over time (see Sec. II C below). As a result, synchronized flow persists during the whole time interval T_{ob} (realization 1 in Fig. 2 (a)).

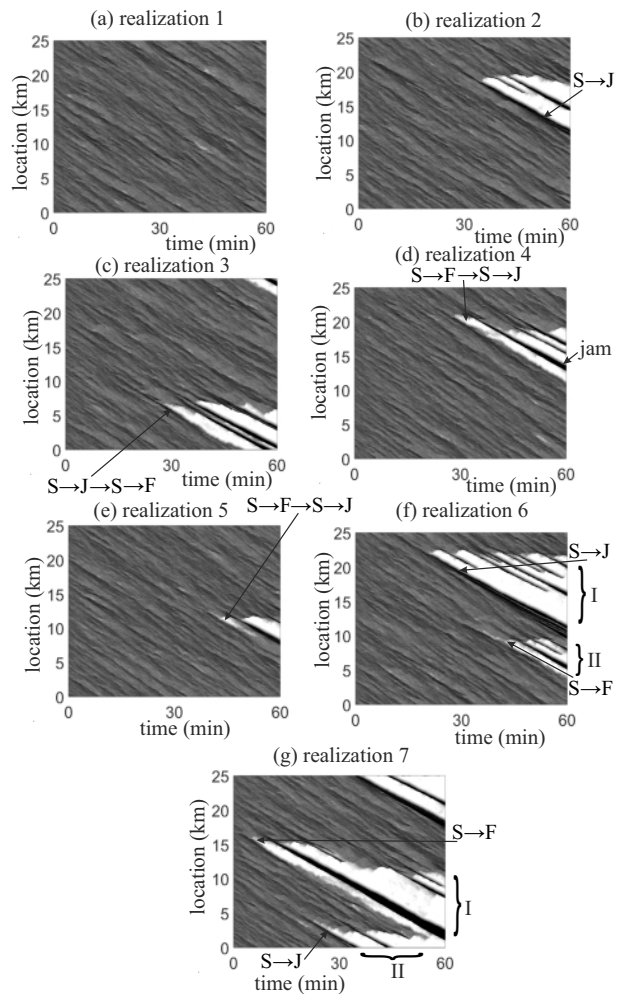


FIG. 2: Characteristic simulation realizations calculated at the same initial state of synchronized flow with $g_{ini} = 19.5$ m, $v_{ini}^{(syn)} = 15$ m/s (54 km/h) and at the same set of model parameters of the KKS model [115]. Vehicle speed data presented by regions with variable shades of gray (shades of gray vary from white to black when the speed decreases from 120 km/h (white) to 0 km/h (black)). Arrows $S \rightarrow F$ label $S \rightarrow F$ transition, arrows $S \rightarrow J$ label $S \rightarrow J$ transition.

- (ii) At some random road location, firstly due to the development of an $S \rightarrow J$ instability, an $S \rightarrow J$ transition occurs (realizations 2, 3, and 6 in Fig. 2 (b, c, f)).
- (iii) At some random road location, firstly due to the development of an $S \rightarrow F$ instability, an $S \rightarrow F$ transition occurs (realizations 4, 5, and 7 in Fig. 2 (d, e, g)).

B. Probabilities of S→F and S→J transitions as functions of average space gap between vehicles in synchronized flow

There is a range of the average space gap \bar{g} (averaged over the circular road) between vehicles in the synchronized flow within which with different probabilities one of the three mentioned basic cases (Sec. II A) of the spatiotemporal competition between S→F and S→J instabilities in synchronized flow occurs randomly (Fig. 3). The average space gap \bar{g} is equal to the chosen initial space gap g_{ini} . Obviously that the space-gap dependencies of the probability $P_S(\bar{g})$ that synchronized flow persists (Fig. 2 (a)), the probability $P_{S_J}(\bar{g})$ that firstly an S→J transition occurs (Fig. 2 (b, c, f)), and the probability $P_{S_F}(\bar{g})$ that firstly an S→F transition occurs (Fig. 2 (d, e, g)) during the time interval T_{ob} satisfy condition:

$$P_S(\bar{g}) + P_{S_F}(\bar{g}) + P_{S_J}(\bar{g}) = 1. \quad (1)$$

From a study of $P_S(\bar{g})$ (Fig. 3 (a)) we have found that

$$P_S(\bar{g}) > 0 \quad \text{only if } g_S < \bar{g} < g_{\text{max}}. \quad (2)$$

Otherwise, outside the space gap range in (2)

$$P_S(\bar{g}) = 0 \quad \text{if } \bar{g} \leq g_S \text{ or } \bar{g} \geq g_{\text{max}}. \quad (3)$$

Under condition (3), during the observation time T_{ob} either an S→F transition or an S→J transition occurs in synchronized flow.

We have found that the probability of the S→F transition $P_{S_F}(\bar{g})$ is an increasing function of \bar{g} (curve P_{S_F} in Fig. 3 (b)). Contrarily, the probability of the S→J transition $P_{S_J}(\bar{g})$ is a decreasing function of \bar{g} (curve P_{S_J} in Fig. 3 (b)) [116]. There is a range of the average space gap \bar{g} within which both $P_{S_F}(\bar{g}) > 0$ and $P_{S_J}(\bar{g}) > 0$:

$$P_{S_F}(\bar{g}) > 0 \text{ and } P_{S_J}(\bar{g}) > 0 \text{ at } g_{\text{min}} < \bar{g} < g_J, \quad (4)$$

where g_{min} and g_J some characteristic values of the average space gap \bar{g} in synchronized flow (Fig. 3 (b)). Within the space gap range (4), randomly either the S→F transition (Fig. 2 (d)) or the S→J transition (Fig. 2 (b)) is possible in synchronized flow. Within the space gap range $g_J \leq \bar{g} < g_{\text{max}}$, $P_{S_J}(\bar{g}) = 0$, therefore, either an S→F transition occurs or synchronized flow persists (Fig. 3).

The probabilities $P_{S_F}(\bar{g})$ (empty circles in Fig. 3 (b)) and $P_{S_J}(\bar{g})$ (black circles in Fig. 3 (b)) are well fitted, respectively, by the functions:

$$P_{S_F}(\bar{g}) = \frac{1}{1 + \exp[-\alpha(\bar{g} - g_p)]}, \quad (5)$$

$$P_{S_J}(\bar{g}) = \frac{1}{1 + \exp[\alpha(\bar{g} - g_p)]}, \quad (6)$$

where α and g_p are parameters (Fig. 3).

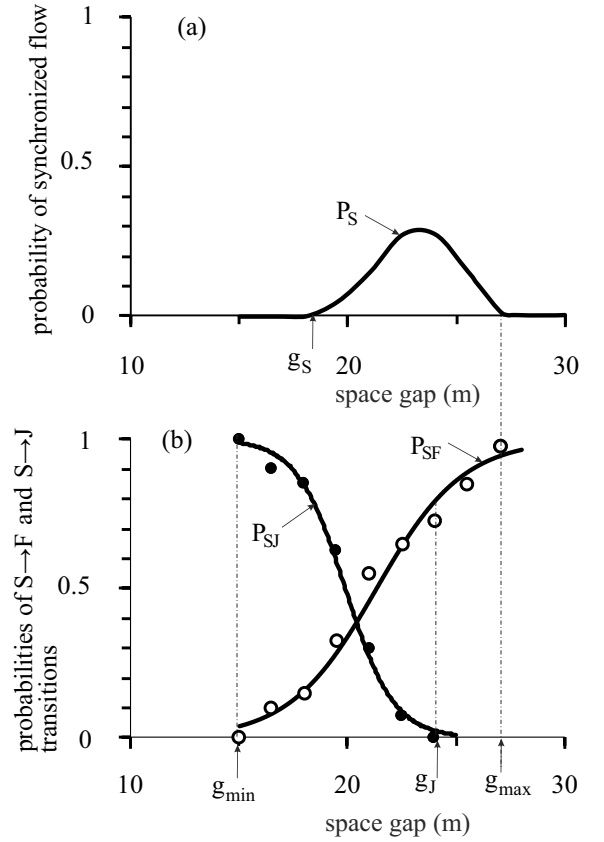


FIG. 3: Probability $P_S(\bar{g})$ (curve P_S) (a) and probabilities $P_{S_F}(\bar{g})$ (curve P_{S_F}), $P_{S_J}(\bar{g})$ (curve P_{S_J}) (b) as functions of $\bar{g} = g_{\text{ini}}$. For calculation of the space-gap functions of the probabilities $P_{S_F}(\bar{g})$ and $P_{S_J}(\bar{g})$, at each given value of g_{ini} different simulation realizations (runs) $N_r = 40$ during the same time interval $T_{\text{ob}} = 60$ min have been made [115]. Then, $P_{S_F}(\bar{g}) = n_r^{(\text{SF})}/N_r$, $P_{S_J}(\bar{g}) = n_r^{(\text{SJ})}/N_r$, where $n_r^{(\text{SF})}$ is the number of realizations in which S→F transition has firstly occurred during the time interval T_{ob} , $n_r^{(\text{SJ})}$ is the number of realizations in which S→J transition has firstly occurred during the time interval T_{ob} . Respectively, $P_S(\bar{g}) = 1 - (P_{S_F}(\bar{g}) + P_{S_J}(\bar{g}))$. Other model parameters are the same as those in Fig. 2. Calculated parameters: $g_{\text{min}} = 15$ m, $g_S = 18$ m, $g_J = 24$ m, $g_{\text{max}} = 27$ m; for function $P_{S_F}(\bar{g})$ (5) parameters $\alpha = 0.52 \text{ m}^{-1}$ and $g_p = 21.1$ m; for function $P_{S_J}(\bar{g})$ (6) parameters $\alpha = 0.9 \text{ m}^{-1}$ and $g_p = 19.6$ m.

C. Nucleation-interruption effects resulting in dissolving speed waves in synchronized flow: S→F→S and S→J→S transitions

In synchronized flow (Fig. 2 (a)), due to random deceleration and acceleration of vehicles, there are many different local speed disturbances (Fig. 4 (a)). Within the disturbances the speed is either smaller (local speed reduction) or larger (local speed increase) than the average synchronized flow speed denoted by $v_{\text{av}}^{(\text{syn})}$.

If a local speed increase is large enough, an S→F instability is realized (labeled by “S→F instability” in Fig. 4

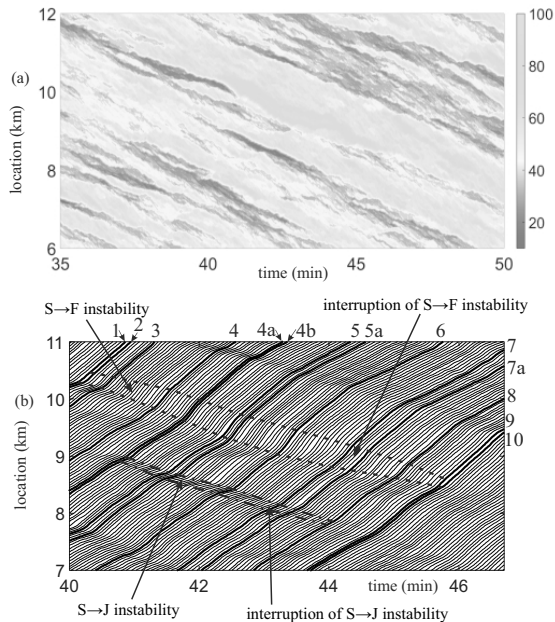


FIG. 4: Continuation of Fig. 2 (a). Dissolving speed waves in synchronized flow: (a) Microscopic speed data presented in space and time. (b) Vehicle trajectories (each 2nd vehicle trajectory is shown). In (b), a region bounded by dashed curves marks S→F instability and its interruption; a region bounded by dashed-dotted curves marks S→J instability and its interruption.

(b)): The maximum speed inside a speed wave caused by this local speed increase begins to grow over time (vehicle trajectories 1–5 in Figs. 4 (b) and 5 (a)).

Respectively, if a local speed decrease is large enough, an S→J instability is realized (labeled by “S→J instability” in Fig. 4 (b)): The minimum speed inside a speed wave caused by this local speed decrease begins to decrease over time (vehicle trajectories 4a, 4b, 5a, 6 in Figs. 4 (b) and 5 (b)); the growing speed wave of the local speed decrease in synchronized flow resulting from the S→J instability is also called a growing narrow moving jam [6].

However, in simulation realization 1 under consideration (Fig. 2 (a)) due to speed adaptation effect that is the same as already explained in [43] no phase transitions occur in synchronized flow. This means that the development of any of the S→F and S→J instabilities that can occur randomly at different road locations are interrupted over time. The interruption of the development of the S→F instability shown in Fig. 5 (a) (trajectories 6–10) leads to a dissolving speed wave of the local speed increase. The interruption of the development of the S→J instability shown in Fig. 5 (b) (trajectories 7a and 8) leads to a dissolving speed wave of the local speed decrease, i.e., the dissolution of the narrow moving jam [6].

In comparison with a known nucleation-interruption

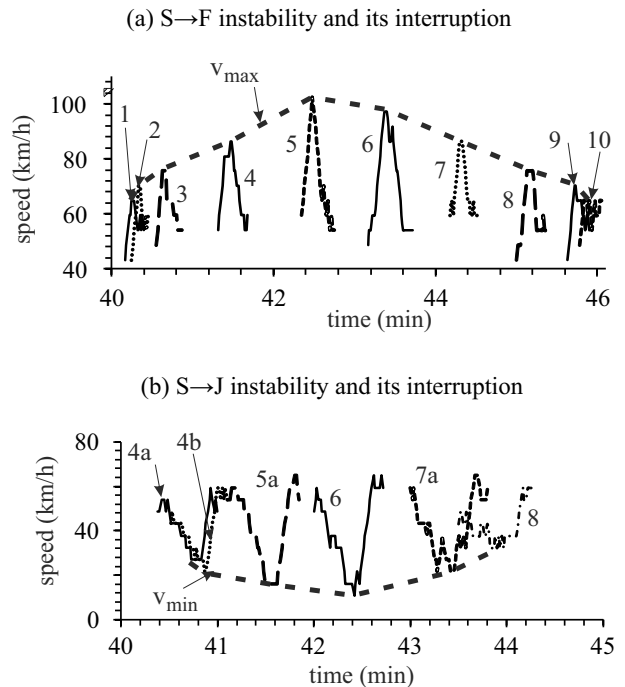


FIG. 5: Continuation of Fig. 4 (b): (a) Fragments of microscopic speeds illustrating S→F instability and its interruption; bold dashed curve $v_{\max}(t)$ shows the time-dependence of the maximum speed on vehicle trajectories. (b) Microscopic speeds illustrating S→J instability and its interruption; bold dashed-dotted curve $v_{\min}(t)$ shows the time-dependence of the minimum speed on vehicle trajectories. Vehicle numbers in (a, b) are the same as those in Fig. 4 (b).

effect of narrow moving jam emergence and dissolution in synchronized flow [6], in the case under consideration due to the competition of the S→F and S→J instabilities, two different nucleation-interruption effects interacting with each other in space and time occur: (i) The emergence with the subsequent dissolution of the speed wave of the local speed increase (Fig. 5 (a)) and (ii) the emergence with the subsequent dissolution of a narrow moving jam (Fig. 5 (b)).

D. S→J instability initiating S→F instability: S→J→S→F transitions

In simulation realization 2 (Fig. 2 (b)), the development of an S→J instability is not interrupted over time; therefore, the development of the S→J instability leads to an S→J transition, i.e., wide moving jam emergence. The microscopic development of this effect can be seen on trajectories 1–5 in Fig. 6 (a) and on trajectories 1–3 in Fig. 7 (a)). The S→J transition (Fig. 7 (a)) is a well-known effect [6]. However, due to the possibility of random occurrence of either S→F instability or S→J instability at the same model parameters, we have revealed nucleation phenomena that have been unknown

up to now (Fig. 6 (b, c)).

1. *S→F instability and its interruption downstream of moving jam*

Because the S→J instability shown in Fig. 6 (a) occurs in synchronized flow, during the emergence of a moving jam, firstly, synchronized flow is realized both upstream and downstream of the moving jam (trajectories 1 and 2 in Figs. 6 (a) and 7 (a)). Vehicles at the downstream jam front start their acceleration from the moving jam to synchronized flow downstream of the moving jam with a random time delay. Therefore, time highway between two vehicles following each other while accelerating at the jam downstream front is a random value.

Due to a random increase in time delay in vehicle acceleration, time headway between two following vehicles accelerating at the jam downstream front can randomly become considerably longer than the mean time headway. For example, this case occurs between vehicles 6 and 7 shown in Fig. 6 (b). In this case, following vehicle 7 accelerates to a higher speed than preceding vehicle 6. While approaching vehicle 6, vehicle 7 must decelerate to the synchronized flow speed of vehicle 6. As a result, a local speed increase appears in synchronized flow just downstream of the moving jam that we call *speed peak* in synchronized flow downstream of moving jam (labeled by “speed peak” on vehicle trajectory 7 in Fig. 7 (b)).

It turns out that due to this speed peak an S→F instability can occur in synchronized flow downstream of the moving jam [114]. An example of such S→F instability initiated by the speed peak on vehicle trajectory 7 is shown in Figs. 6 (b) and 7 (b): The maximum speed v_{\max} of following vehicles 8 and 9 in Fig. 7 (b) increases. However, in the case under consideration, the development of the S→F instability is interrupted. Therefore, a dissolving speed wave of the local speed increase in synchronized flow is realized (wave labeled by dashed curves in Fig. 6 (b)). This is qualitatively the same effect of the occurrence of a dissolving speed wave of the local speed increase in synchronized flow as that shown in Fig. 5 (a) (Sec. II C). However in contrast with Fig. 5 (a), in the case, the dissolving speed wave of the local speed increase in synchronized flow occurs downstream of a moving jam (Figs. 6 (b) and 7 (b)).

2. *S→F instability resulting in S→F transition downstream from moving jam*

However, in many other cases a speed peak occurring due to a random increase in time delay in vehicle acceleration at the downstream front of a moving jam can randomly become large enough to cause an S→F transition. For example, such a long time delay occurs between vehicles 12 and 13 shown in Figs. 6 (c) and 7 (c). As a result, a growing speed wave of the local speed increase

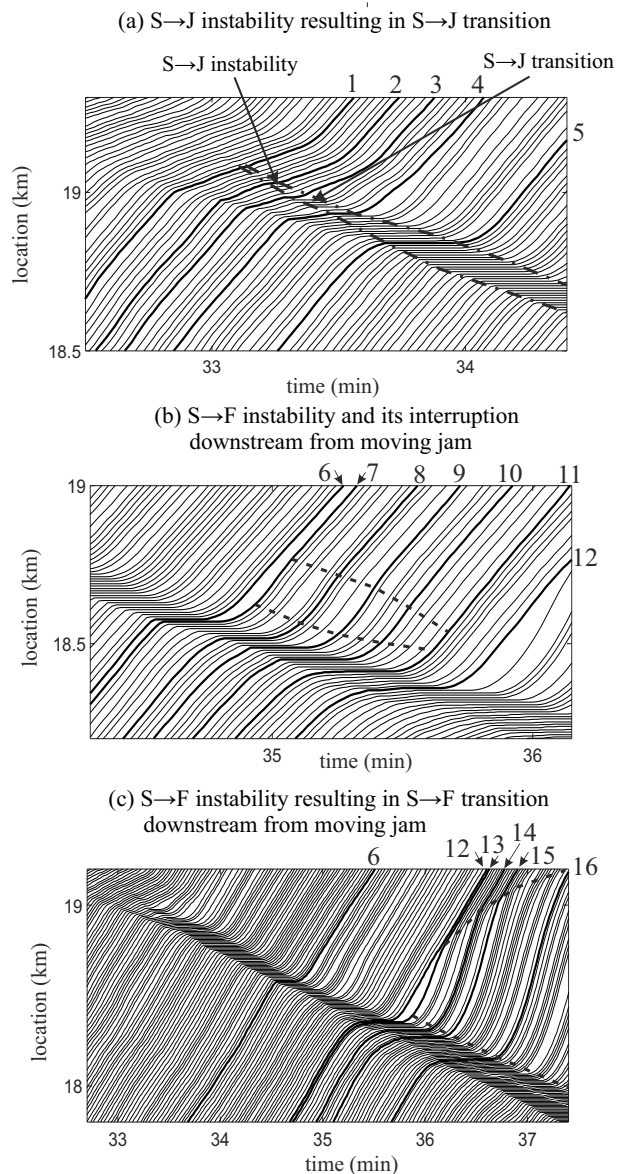


FIG. 6: Continuation of Fig. 2 (b). S→J instability and resulting spatiotemporal nucleation traffic phenomena in synchronized flow: (a) Vehicle trajectories illustrating S→J instability resulting in S→J transition. (b) Vehicle trajectories for a later time interval as that in (a); illustration of S→F instability and its interruption downstream of moving jam resulting from the development of the S→J instability shown in (a). (c) Vehicle trajectories for a longer time interval as that in (a); illustration of S→F instability that leads to S→F transition downstream of moving jam resulting from the development of the S→J instability shown in (a).

in synchronized flow is realized (wave labeled by dashed curves in Fig. 6 (c)). In this case, the development of an S→F instability leads to an S→F transition (speed of vehicle 16 reaches the maximum free flow speed v_{free} in Fig. 7 (c)).

Thus, in this case the initial S→J instability leads

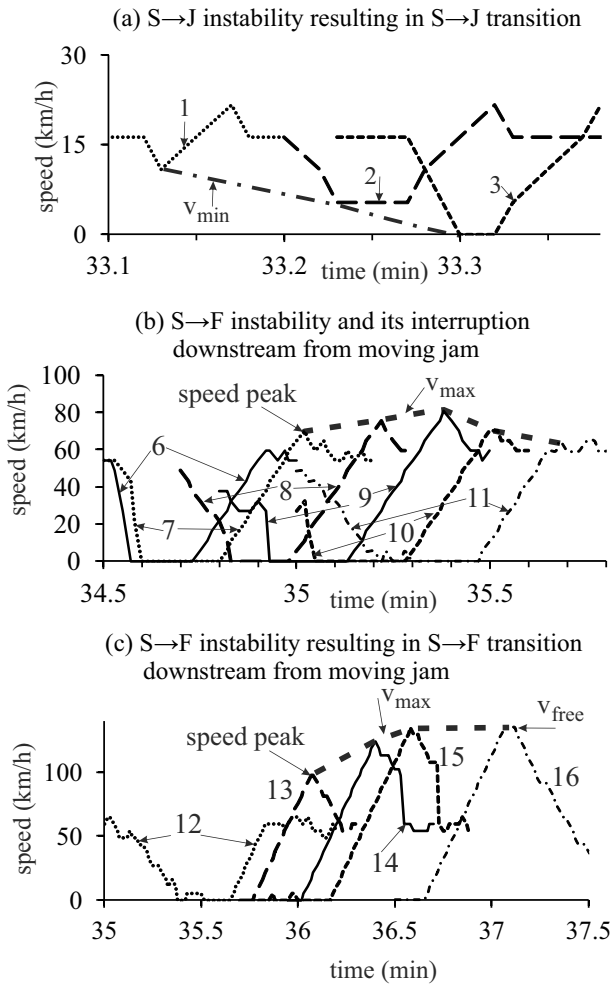


FIG. 7: Continuation of Fig. 6: (a) Fragments of microscopic speeds related to Fig. 6 (a); bold dashed-dotted curve $v_{\min}(t)$ shows the time-dependence of the minimum speed on vehicle trajectories; vehicle numbers in (a) are the same as those in Fig. 6 (a). (b) Fragments of microscopic speeds related to Fig. 6 (b); bold dashed curve $v_{\max}(t)$ shows the time-dependence of the maximum speed on vehicle trajectories; vehicle numbers in (b) are the same as those in Fig. 6 (b). (c) Fragments of microscopic speeds related to Fig. 6 (c); bold dashed curve $v_{\max}(t)$ shows the time-dependence of the maximum speed on vehicle trajectories; vehicle numbers in (c) are the same as those in Fig. 6 (c).

firstly to S→J transition (labeled by “S→J transition” in Fig. 6 (a)); later, due to a random time delay in vehicle acceleration at the downstream jam front, a speed peak occurs in synchronized flow downstream of the moving jam (Fig. 7 (c)); the speed peak initiates the S→F instability; the development of the S→F instability results in the S→F transition (labeled by dashed curves in Figs. 6 (c) and 7 (c)). In other words, the initial S→J instability causes a sequence of S→J→S→F transitions.

There are simulation realizations in which sequences of S→J→S→F transitions can exhibit some other features.

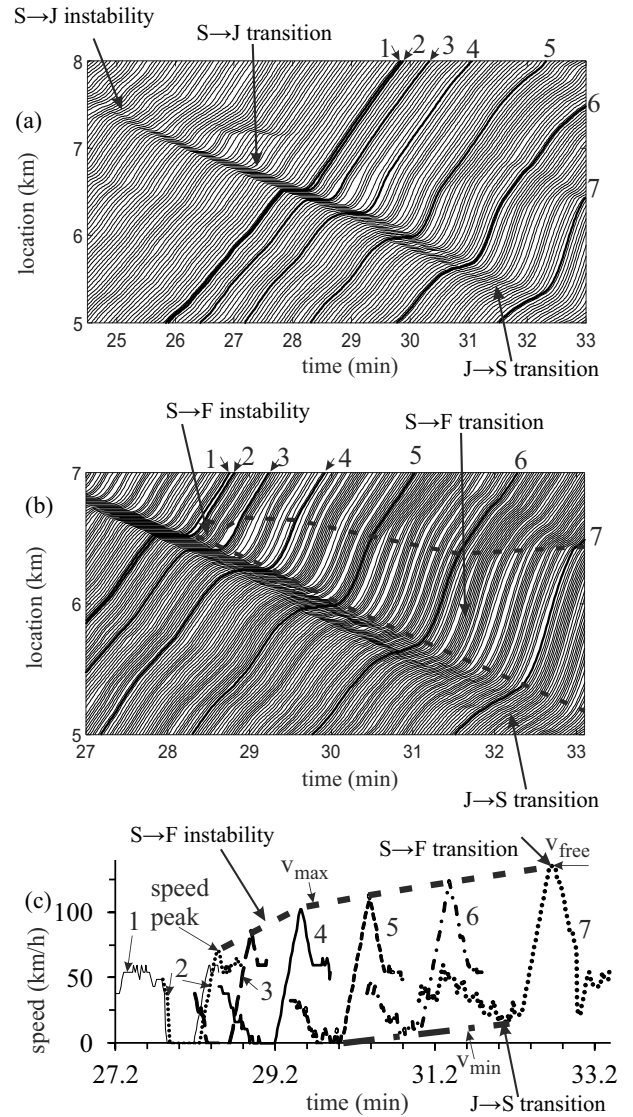


FIG. 8: Continuation of Fig. 2 (c): S→J instability resulting in S→J transition with subsequent S→F transition downstream of the moving jam following by jam dissolution (J→S transition): (a, b) Vehicle trajectories for different time intervals; in (a) each 2nd trajectory and in (b) each trajectory are shown. (c) Fragments of microscopic speeds illustrating S→F transition downstream of moving jam and jam dissolution (J→S transition); bold dashed and dashed-dotted curves $v_{\max}(t)$ and $v_{\min}(t)$ show, respectively, the time-dependence of the maximum and minimum speeds on vehicle trajectories. Vehicle numbers in (c) are the same as those in (a, b).

An example is shown in Fig. 8. Firstly, as in Fig. 6, an initial S→J instability leads to S→J transition (labeled by “S→J transition” in Fig. 8 (a)). Then, a speed peak occurs in synchronized flow downstream of the moving jam (Fig. 8 (c)). The speed peak initiates the S→F instability that development results in the S→F transition (Fig. 8 (c)). Consequently, a sequence of S→J→S→F transi-

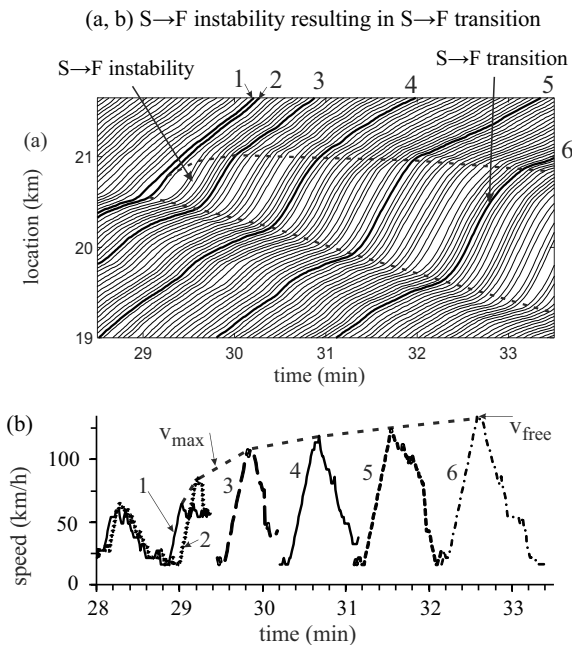


FIG. 9: Continuation of Fig. 2 (d). $S \rightarrow F$ instability resulting in $S \rightarrow F$ transition: (a) Vehicle trajectories. (b) Fragments of microscopic speeds illustrating $S \rightarrow F$ instability resulting in $S \rightarrow F$ transition; bold dashed curve $v_{\max}(t)$ shows the time-dependence of the maximum speed on vehicle trajectories. Vehicle numbers in (b) are the same as those in (a).

tions is realized. However, in contrast with the sequence of $S \rightarrow J \rightarrow S \rightarrow F$ transitions shown in Figs. 6 and 7, in the case under consideration (Fig. 8) due to the speed adaptation effect at the upstream jam front the wide moving jam dissolves over time and synchronized flow returns (labeled by “ $J \rightarrow S$ transition” in Figs. 8 (a-c)).

E. $S \rightarrow F$ instability leading to $S \rightarrow F$ transition

An $S \rightarrow F$ transition can also randomly occur in synchronized flow without the effect of a moving jam discussed in Sec. IID 2. This case is shown in simulation realization 4 (Fig. 2 (d)): A large enough local speed increase in synchronized flow appears randomly initiating an $S \rightarrow F$ instability. The development of the $S \rightarrow F$ instability is not interrupted over time; therefore, the development of the $S \rightarrow F$ instability leads to an $S \rightarrow F$ transition. The microscopic development of this effect is shown in Fig. 9.

Within a road region of the development of the $S \rightarrow F$ instability, the vehicle speed increases subsequently over time. Because synchronized flow exists downstream of this local region, vehicles must decelerate approaching slower moving vehicles ahead. This results in a speed wave within which the speed is larger than in surrounded synchronized flow (trajectories 2–4 in Fig. 9). The subsequent growth of this wave causes the $S \rightarrow F$ transition

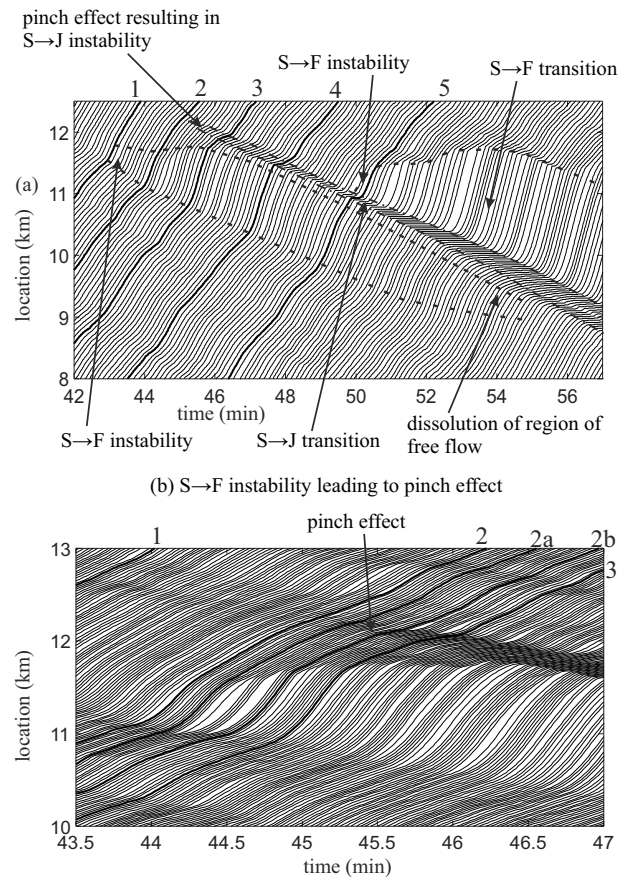


FIG. 10: Continuation of Fig. 2 (e). $S \rightarrow F$ instability resulting in $S \rightarrow J$ transition: (a) Vehicle trajectories; each 4th vehicle trajectory is shown. (b) Vehicle trajectories; each vehicle trajectory is shown.

(trajectories 5, 6 in Fig. 9).

F. $S \rightarrow F$ instability initiating $S \rightarrow J$ instability: $S \rightarrow F \rightarrow S \rightarrow J$ transitions

It turns out that when due to an $S \rightarrow F$ instability a growing speed wave of a local speed increase is realized, then due to a time delay in vehicle deceleration, vehicles decelerating at the downstream front of this growing speed wave come on average at small space gaps to each other. As a result, the pinch effect can occur in synchronized flow that leads to an $S \rightarrow J$ instability (emergence of a growing narrow moving jam(s)) resulting in an $S \rightarrow J$ transition (Figs. 10 and 11). Thus, when the initial $S \rightarrow F$ instability causes the pinch effect downstream of the growing speed wave of a local speed increase in synchronized flow, this $S \rightarrow F$ instability can cause a sequence of phase transitions that can be called as $S \rightarrow F \rightarrow S \rightarrow J$ transitions.

The development of the sequence of $S \rightarrow F \rightarrow S \rightarrow J$ transitions is as follows. The flow rate in synchronized flow

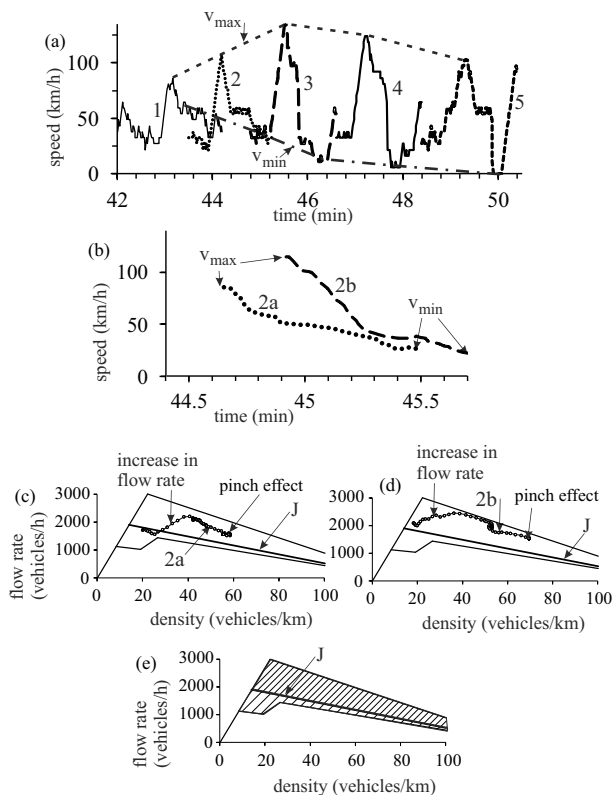


FIG. 11: Continuation of Fig. 10. (a) Fragments of microscopic speeds; bold dashed and dashed-dotted curves $v_{\max}(t)$ and $v_{\min}(t)$ show, respectively, the time-dependence of the maximum and minimum speeds on vehicle trajectories; vehicle numbers in (a) are the same as those in Fig. 10 (a). (b) Fragments of microscopic speeds of vehicles shown by the same numbers in Fig. 10 (b). (c, d) Points along vehicle trajectories 2a (c) and 2b (d) in the flow-density plane; averaging over 10 vehicles upstream of the related vehicle for each time step (1 sec). (e) Explanation of the pinch effect [6]: Points on and above the line J are metastable with respect to $S \rightarrow J$ transition; points below the line J are stable with respect to $S \rightarrow J$ instability.

increases considerably just downstream of the growing wave of the local speed increase caused by the $S \rightarrow F$ instability (labeled by “increase in flow rate” on trajectories 2a and 2b in Figs. 11 (c, d)). As known from other studies of dense synchronized flow (Fig. 11 (e)) [6, 48], due to the flow rate increase in synchronized flow the pinch effect is often realized: The density of synchronized flow increases considerably and the speed decreases while points related to the synchronized flow remain to be above the line J in the flow-density plane (labeled by “pinch effect” on points related to vehicles 2a and 2b in Figs. 11 (c, d)). The narrow moving jam that has emerged in the pinch region of synchronized flow transforms in a wide moving jam. Thus, the initial $S \rightarrow F$ instability causes both the emergence of the local region of a higher speed and, as the subsequent effect, the $S \rightarrow J$ instability resulting in the $S \rightarrow J$ transition.

In the example shown in Fig. 10, the growing speed wave of the local speed increase ($S \rightarrow F$ instability), which has led to the pinch effect resulting in the $S \rightarrow J$ transition, transforms into a dissolving speed wave of a local speed increase. Indeed, the local region of free flow dissolves over time (labeled by “dissolution of region of free flow” in Fig. 10 (a)).

However, the pinch effect caused by the $S \rightarrow F$ instability is often also observed even when a local region of free flow resulting from the initial $S \rightarrow F$ instability does not dissolve over time. An example is a sequence of $S \rightarrow F \rightarrow S \rightarrow J$ transitions (labeled by “ $S \rightarrow F \rightarrow S \rightarrow J$ ” in Fig. 2 (d)) caused by the $S \rightarrow F$ instability discussed in Sec. II E. In this sequence of $S \rightarrow F \rightarrow S \rightarrow J$ transitions the resulting wide moving jam is labeled by “jam” in Fig. 2 (d).

G. Independent development of both $S \rightarrow F$ and $S \rightarrow J$ transitions in the same simulation realization

In Fig. 2 (b–e), we have observed different realizations simulated at the same model parameters. We have found that after an $S \rightarrow F$ transition has occurred a subsequent (secondary) $S \rightarrow J$ transition is possible (called as $S \rightarrow F \rightarrow S \rightarrow J$ transitions) (Sec. II F); respectively, after an $S \rightarrow J$ transition has occurred a subsequent (secondary) $S \rightarrow F$ transition is possible (called as $S \rightarrow J \rightarrow S \rightarrow F$ transitions) (Sec. II D). In both cases, the secondary phase transition depends on the development of the initial one. However, simulations show that due to the competition between the $S \rightarrow F$ and $S \rightarrow J$ instabilities in initial synchronized flow, in other realizations the independent development of $S \rightarrow F$ and $S \rightarrow J$ transitions in different sections of the road at different random time instants is also possible (Fig. 2 (f, g)).

In realization 6 (Fig. 2 (f)), earlier an $S \rightarrow J$ instability has occurred. As a result, a region (labeled by bracket I) in which complex spatiotemporal alternations of wide moving jams, free flow, and synchronized flow are formed occurs; later in the synchronized flow outside this region, due to an $S \rightarrow F$ instability other alternations of traffic phases J , S , and F are formed (labeled by bracket II in Fig. 2 (f)). Similar phenomena are observed in realization 7 (Fig. 2 (g)). In this case, earlier through the development of an $S \rightarrow F$ instability alternations of traffic phases J , S , and F are formed (labeled by bracket I in Fig. 2 (g)); later another region of alternations of traffic phases J , S , and F is realized randomly (labeled by bracket II).

III. PROBABILISTIC FEATURES OF COMPETITION BETWEEN $S \rightarrow F$ AND $S \rightarrow J$ INSTABILITIES AT HIGHWAY BOTTLENECK

In real traffic, synchronized flow occurs usually at bottlenecks. In this section, we show that the statistical physics of synchronized flow presented in Sec. II can ex-

plain statistical features of synchronized flow at road bottlenecks. For simplicity, we consider synchronized flow at an on-ramp bottleneck on a single-lane road. Our simulations have shown that results of this analysis remain qualitatively for other bottleneck types. It is known that synchronized flow at the bottleneck occurs due to a spontaneous $F \rightarrow S$ transition that exhibits a random time delay [6]. The physics of a random time delay is explained by a sequence of random $F \rightarrow S \rightarrow F$ transitions at the bottleneck [43]. Because the $F \rightarrow S \rightarrow F$ transitions have already been studied [43], in simulations rather than a spontaneous $F \rightarrow S$ transition, synchronized flow at the bottleneck that statistical features should be studied results from an induced $F \rightarrow S$ transition (Fig. 12). To induce the $F \rightarrow S$ transition, in all simulation realizations presented in Fig. 12 we apply the same on-ramp inflow impulse of the amplitude $q_{\text{on}}^{(\text{imp})} = 795$ vehicles/h within time interval $0 \leq t \leq 4$ min; at $t > 4$ min a given on-ramp inflow rate q_{on} is time-independent.

A. Probabilities of $S \rightarrow F$ and $S \rightarrow J$ transition at bottleneck as functions of flow rate

At the same model parameters and the same values of the flow rate in free flow upstream of the bottleneck q_{in} and the on-ramp inflow rate q_{on} , there are a number of simulation realizations in which different spatiotemporal critical traffic phenomena in synchronized flow at the bottleneck have been found. Characteristic simulation realizations are shown in Fig. 12.

We have found that due to the spatiotemporal competition between $S \rightarrow F$ and $S \rightarrow J$ instabilities in synchronized flow there is a range of the flow rate q_{sum} within which during the observation time T_{ob} either synchronized flow persists (Fig. 12 (a)), or firstly an $S \rightarrow J$ transition occurs in synchronized flow (Fig. 12 (b, c, f)), or else firstly an $S \rightarrow F$ transition occurs in synchronized flow (Fig. 12 (d, e, g)) with different probabilities, respectively, $P_S(q_{\text{sum}})$, $P_{SJ}(q_{\text{sum}})$, and $P_{SF}(q_{\text{sum}})$. Here and below the flow rate q_{sum} is equal to

$$q_{\text{sum}} = q_{\text{on}} + q_{\text{in}}. \quad (7)$$

It has been found that the flow rate dependencies of these probabilities $P_S(q_{\text{sum}})$, $P_{SJ}(q_{\text{sum}})$, and $P_{SF}(q_{\text{sum}})$ (Fig. 13) are qualitatively the same as those for a homogeneous road (Fig. 3) found in Sec. II. Respectively, if the average space gap \bar{g} in formulas (1)–(4) is replaced by the flow rate q_{sum} , then we come to formula $P_S(q_{\text{sum}}) + P_{SF}(q_{\text{sum}}) + P_{SJ}(q_{\text{sum}}) = 1$ as well as formulas

$$P_S(q_{\text{sum}}) > 0 \quad \text{only if } q_{\text{sum}}^{(\text{min})} < q_{\text{sum}} < q_{\text{sum}}^{(\text{S})}, \quad (8)$$

$$P_S(q_{\text{sum}}) = 0 \quad \text{if } q_{\text{sum}} \leq q_{\text{sum}}^{(\text{min})} \text{ or } q_{\text{sum}} \geq q_{\text{sum}}^{(\text{S})}, \quad (9)$$

$$P_{SF}(q_{\text{sum}}) > 0 \text{ and } P_{SJ}(q_{\text{sum}}) > 0 \text{ at } q_{\text{sum}}^{(\text{J})} < q_{\text{sum}} < q_{\text{sum}}^{(\text{max})}. \quad (10)$$

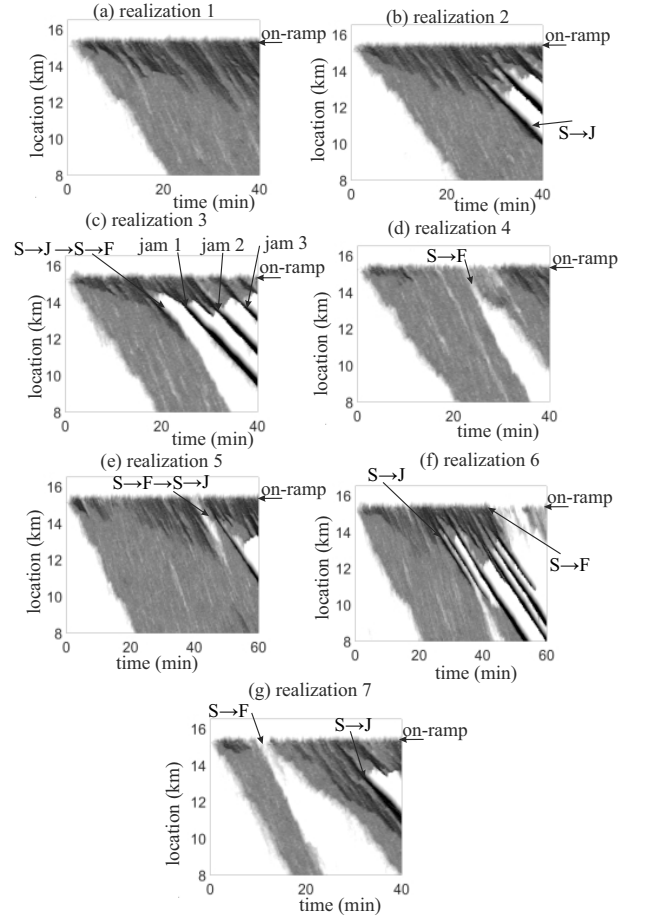


FIG. 12: Characteristic simulation realizations of synchronized flow at on-ramp bottleneck calculated at the same set of parameters of the KKS model, parameters of on-ramp bottleneck, and of the flow rates [115]: Vehicle speed data presented by regions with variable shades of gray (shades of gray vary from white to black when the speed decreases from 120 km/h (white) to 0 km/h (black)). $q_{\text{in}} = 1914$ vehicles/h. $q_{\text{on}} = 374$ vehicles/h. The beginning and end of the on-ramp merging region are, respectively, $x_{\text{on}} = 15$ and $x_{\text{on}}^{(\text{e})} = 15.3$ km. Arrows $S \rightarrow F$ label $S \rightarrow F$ transition, arrows $S \rightarrow J$ label $S \rightarrow J$ transition.

Formulas (8)–(10) determine some characteristic flow rates $q_{\text{sum}}^{(\text{S})}$, $q_{\text{sum}}^{(\text{min})}$, $q_{\text{sum}}^{(\text{max})}$, and $q_{\text{sum}}^{(\text{J})}$ (Fig. 13). These characteristic flow rates have qualitatively the same sense as the characteristic average space gaps in synchronized flow on a homogeneous road in formulas (2)–(4) (Sec. II).

The flow-rate function of the probability $P_{SF}(q_{\text{sum}})$ (empty circles in Fig. 13 (b)) is well fitted by a function:

$$P_{SF}(q_{\text{sum}}) = \frac{1}{1 + \exp[\alpha(q_{\text{sum}} - q_0)]}; \quad (11)$$

respectively, the flow-rate function of the probability $P_{SJ}(q_{\text{sum}})$ (black circles in Fig. 13 (b)) is well fitted by a

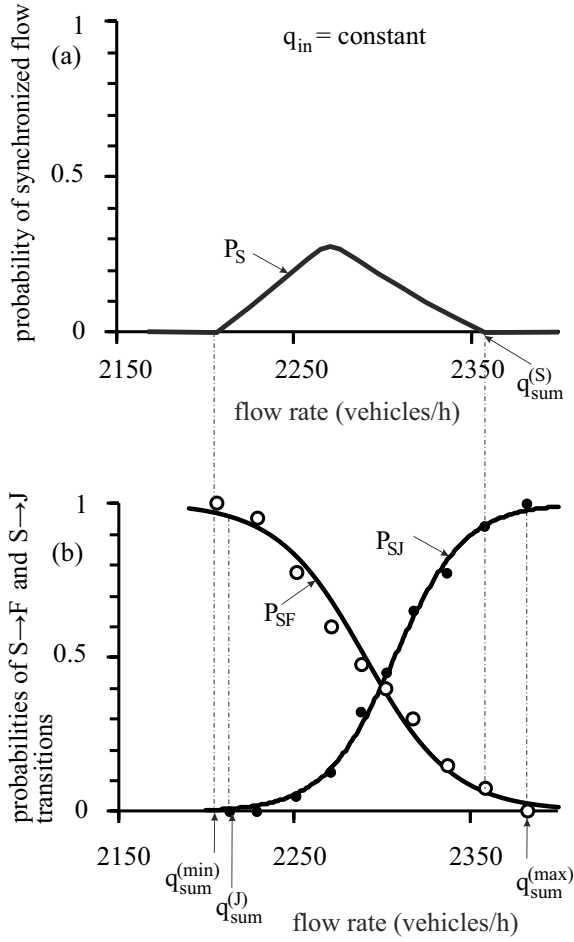


FIG. 13: Probabilities $P_S(q_{\text{sum}})$ (curve P_S) (a) and $P_{SF}(q_{\text{sum}})$ (curve P_{SF}), $P_{SJ}(q_{\text{sum}})$ (curve P_{SJ}) (b) as functions of the flow rate $q_{\text{sum}} = q_{\text{on}} + q_{\text{in}}$ calculated through the change in q_{on} at given flow rate $q_{\text{in}} = 1914$ vehicles/h. For calculation of $P_{SF}(q_{\text{sum}})$ and $P_{SJ}(q_{\text{sum}})$, at each given value of q_{sum} different simulation realizations (runs) $N_r = 40$ during the time interval $T_{\text{ob}} = 40$ min at the same set of model parameters [115] have been calculated. $P_{SF}(q_{\text{sum}}) = n_r^{(SF)}/N_r$, $P_{SJ}(q_{\text{sum}}) = n_r^{(SJ)}/N_r$, where $n_r^{(SF)}$ is the number of realizations in which $S \rightarrow F$ transition has firstly occurred during the time interval T_{ob} , $n_r^{(SJ)}$ is the number of realizations in which $S \rightarrow J$ transition has firstly occurred during the time interval T_{ob} ; respectively, $P_S(q_{\text{sum}}) = 1 - (P_{SF}(q_{\text{sum}}) + P_{SJ}(q_{\text{sum}}))$. Other model parameters are the same as those in Fig. 12. Calculated values: $q_{\text{sum}}^{(\text{min})} = 2206$, $q_{\text{sum}}^{(J)} = 2213$, $q_{\text{sum}}^{(S)} = 2358$, $q_{\text{sum}}^{(\text{max})} = 2382$ vehicles/h; $\alpha = 0.04$ h/vehicles and $q_0 = 2290$ vehicles/h in (11), $\alpha = 0.05$ h/vehicles and $q_0 = 2307$ vehicles/h in (12).

function:

$$P_{SJ}(q_{\text{sum}}) = \frac{1}{1 + \exp[-\alpha(q_{\text{sum}} - q_0)]}, \quad (12)$$

where q_{sum} is the flow rate at the bottleneck (7), α and q_0 are constants (Fig. 13).

As we can see, probabilistic features of synchronized

flow at the bottleneck (Fig. 13) are qualitatively the same as those on a homogeneous road (Fig. 3). However, there is a basic difference between these two cases: On a homogeneous road, critical local disturbances initiating the $S \rightarrow F$ and $S \rightarrow J$ instabilities appear at random road locations. On contrarily, as well-known the bottleneck introduces a large local inhomogeneity in traffic. For this reason, one can expect that critical local disturbances should appear randomly mostly in a vicinity of the bottleneck. Although this conclusion is obvious from earlier studies of traffic at a bottleneck [6, 43], as we will see below, due to the competition of $S \rightarrow F$ and $S \rightarrow J$ instabilities a number of unknown before spatiotemporal traffic phenomena can be found at a bottleneck.

B. Effect of competition of $S \rightarrow F$ and $S \rightarrow J$ instabilities on speed waves in synchronized flow at bottleneck

Speed (and, respectively, density) waves in synchronized flow caused either by the $S \rightarrow J$ instability [6] or by the $S \rightarrow F$ instability [43] are known. It has been unknown that due to the competition of $S \rightarrow F$ and $S \rightarrow J$ instabilities at the bottleneck, in the same realization random alternations of these both instabilities can occur leading to speed and density waves in synchronized flow that are non-regular in space and time (Fig. 14) [117].

In particular, these waves occur through the effect of an $S \rightarrow F$ instability and its interruption as well as the effect an $S \rightarrow J$ instability and its interruption occurring randomly at the bottleneck at different time instants as shown, respectively, in Fig. 15 (a, b) and Fig. 15 (c, d). To find the reason for the alternation of these two different effects, we should consider initial local speed disturbances occurring due to vehicle merging from the on-ramp onto the main road within the on-ramp merging region ($15.3 \text{ km} \leq x \leq 15 \text{ km}$) at the bottleneck (Fig. 15 (a, c)). There are two qualitatively different kinds of the initial local disturbances: (i) ‘‘Speed peak’’ (Fig. 15 (b)) occurs due to the merging of vehicle 2 from on-ramp (dotted curves 2 in Figs. 15 (a, b)): The motion of downstream vehicle 1 is not influenced by vehicle 2. It is different for upstream vehicle 3, which has earlier accelerated while following vehicle 1; after the merging of vehicle 2, vehicle 3 must interrupt its acceleration and decelerate strongly to avoid the collision with vehicle 2 [43]. (ii) ‘‘Local speed reduction’’ (Fig. 15 (d)) occurs also due to the merging of vehicle 9 from on-ramp (dotted curves 9 in Figs. 15 (c, d)); in this case, in contrast with the speed peak, upstream vehicle 10 has not still earlier accelerated behind vehicle 8, therefore, vehicle 10, while decelerating behind slow moving vehicle 9, produces no speed peak [6].

These different disturbances at the bottleneck cause two different effects: 1. The speed peak initiates an $S \rightarrow F$ instability: A speed wave of local speed increase grows while propagating upstream (trajectories 3–5 in Fig. 15 (b)); however, in the case under consideration the devel-

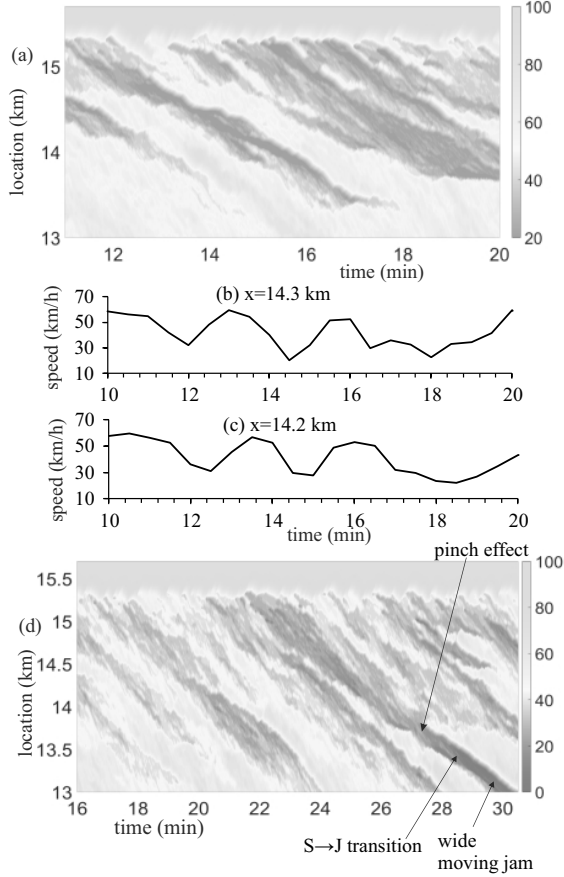


FIG. 14: Waves in synchronized flow at bottleneck: (a) Fragment of vehicle speed data presented by regions with variable shades of gray related to Fig. 12 (a). (b, c) Time-functions of average speed (30 sec averaged data) measured by virtual detectors at two different locations in (a). (d) Fragment of vehicle data presented by regions with variable shades of gray related to Fig. 12 (b). In (a, d), the beginning and end of the on-ramp merging region are, respectively, $x_{\text{on}} = 15$ and $x_{\text{on}}^{(e)} = 15.3$ km.

opment of the S→F instability is interrupted (trajectories 5–7 in Fig. 15 (b)) and, therefore, no S→F transition occurs. 2. The local speed reduction initiates an S→J instability: A speed wave of local speed decrease (narrow moving jam) grows while propagating upstream (trajectories 10 and 11 in Fig. 15 (d)); however, in the case under consideration the development of the S→J instability is interrupted (trajectories 11–14 in Fig. 15 (d)) and, therefore, no wide moving jam (S→J transition) occurs. In Fig. 14 (a), all speed waves dissolve over time (dissolving speed waves), i.e., neither S→F transition nor S→J transition is realized.

In some realizations, within a dissolving wave of the local speed increase in synchronized flow randomly a local increase in the speed can appear at some distance upstream of the bottleneck causing an S→F transition. Such cases associated with the dissolving wave found in

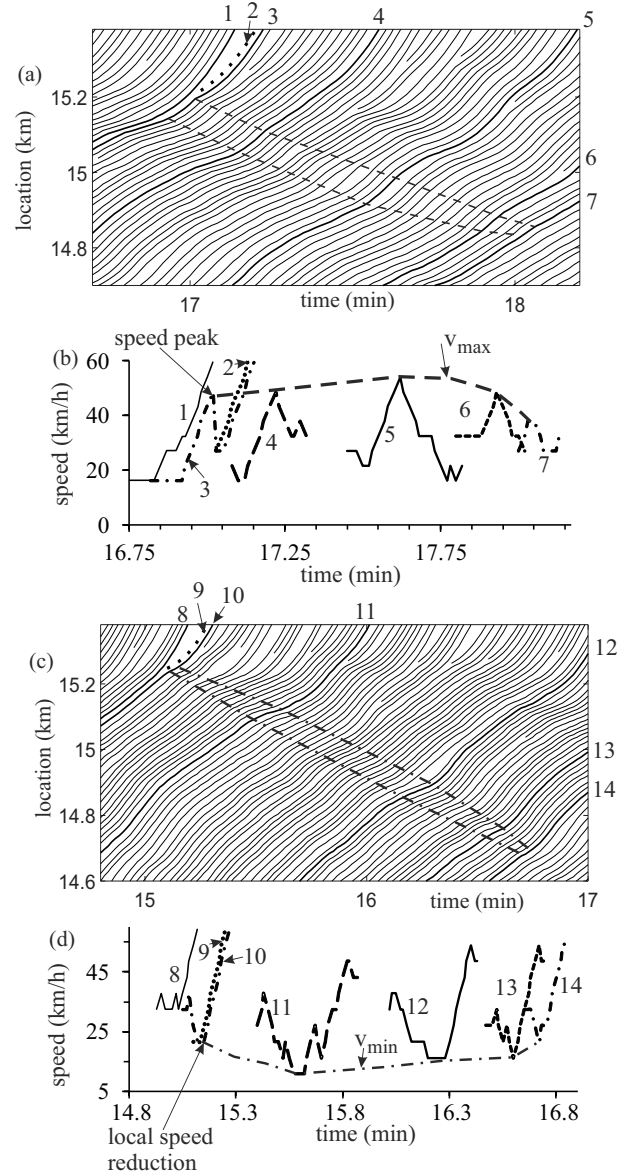


FIG. 15: Continuation of Fig. 14 (a): (a, b) S→F instability and its interruption. (c, d) S→J instability and its interruption. (a, c) Fragments of vehicle trajectories. (b, d) Fragments of time-functions of microscopic speeds for different vehicles whose numbers are the same as those in (a, c), respectively. In (a, c), the beginning and end of the on-ramp merging region are, respectively, $x_{\text{on}} = 15$ and $x_{\text{on}}^{(e)} = 15.3$ km.

simulations are not shown. This is because such cases are relatively seldom. In the other realizations, in which a speed peak appears just at the bottleneck location while initiating an S→F instability, the development of the S→F instability leads to an S→F transition (Figs. 12 (d, e, f, g)) as already studied in [43]. However, as found in this paper rather than the latter known scenario of the development of the S→F transition [43], many of the S→F transitions that occur upstream of the bottleneck

result from a qualitatively different scenario: These $S \rightarrow F$ transitions are the consequence of initial $S \rightarrow J$ instabilities leading to sequences of $S \rightarrow J \rightarrow S \rightarrow F$ transitions (see Sec. III C).

In some other realizations, within a wave of the local speed decrease in synchronized flow randomly the pinch effect is realized at a considerable distance upstream of the bottleneck. Such a case of the pinch effect with the subsequent $S \rightarrow J$ transition is shown in Fig. 14 (d). In other realizations, an $S \rightarrow J$ instability (pinch effect with growing narrow moving jams) occurs just at the bottleneck location (Figs. 12 (c, f, g)); in these cases, the $S \rightarrow J$ instability leads to an $S \rightarrow J$ transition as already studied in [6]. However, as found in this paper rather than the latter well-known scenario of the development of the $S \rightarrow J$ transition [6], many of the $S \rightarrow J$ transitions that occur upstream of the bottleneck result from a qualitatively different scenario: These $S \rightarrow J$ transitions are the consequence of initial $S \rightarrow F$ instabilities leading to sequences of $S \rightarrow F \rightarrow S \rightarrow J$ transitions (see Sec. III D).

C. $S \rightarrow J \rightarrow S \rightarrow F$ transitions at bottleneck

Sequences of $S \rightarrow J \rightarrow S \rightarrow F$ transitions found for a homogeneous road (Sec. II D) are often observed in synchronized flow at the bottleneck.

An example of $S \rightarrow J \rightarrow S \rightarrow F$ transitions in synchronized flow at the bottleneck is presented in Fig. 16. As for the homogeneous road (Fig. 8), a moving jam that emerges due to the development of an $S \rightarrow J$ instability in synchronized flow at the bottleneck results in an $S \rightarrow F$ instability with the subsequent an $S \rightarrow F$ transition downstream of the moving jam (Fig. 16) [119]. As on homogeneous road (Fig. 8), the wide moving jam dissolves over time (Fig. 16 (b, c)). However, it should be emphasized that such a jam dissolution (Fig. 16 (b, c)) is not a general case: In other cases of the occurrence of a sequence of $S \rightarrow J \rightarrow S \rightarrow F$ transitions at the bottleneck, both the wide moving jam and free flow downstream of the moving jam persist over time. This is realized even in the same realization 3 (persisting wide moving jams are labeled by “jam 1”, “jam 2”, and “jam 3” in Fig. 12 (c)).

The similarity of $S \rightarrow J \rightarrow S \rightarrow F$ transitions at the bottleneck and on the homogeneous road is explained as follows: After a moving jam has occurred in synchronized flow at the bottleneck, the subsequent development of an $S \rightarrow F$ instability downstream of the moving jam occurs far upstream of the bottleneck. Therefore, this $S \rightarrow F$ instability does not almost depend on the bottleneck: The bottleneck is the reason for synchronized flow occurrence. After synchronized flow has already occurred at the bottleneck, further critical phenomena in synchronized flow like $S \rightarrow J \rightarrow S \rightarrow F$ transitions are qualitatively the same for a hypothetical homogeneous road and for real roads with bottlenecks.

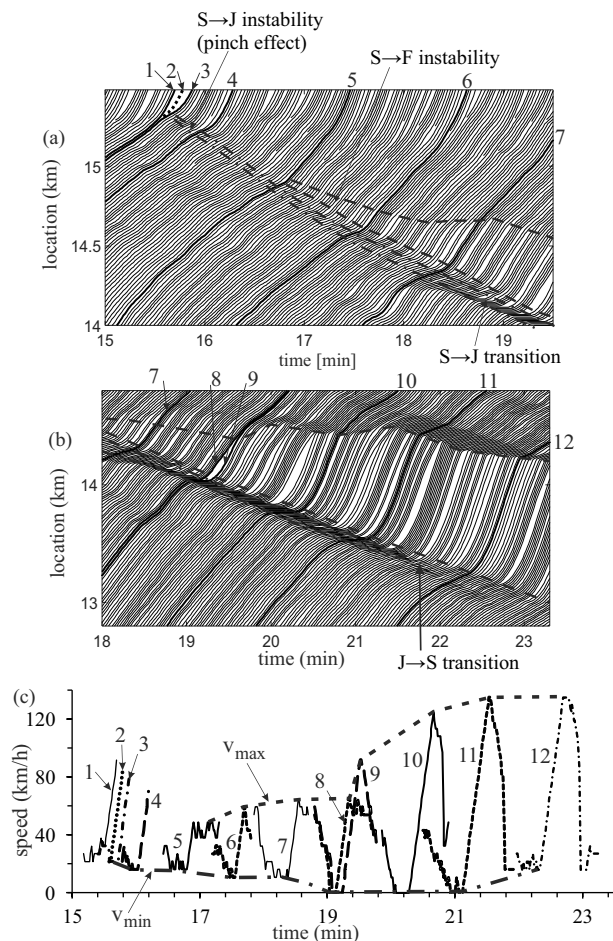


FIG. 16: Continuation of Fig. 12 (c). $S \rightarrow J \rightarrow S \rightarrow F$ transitions at bottleneck: (a, b) Fragments of vehicle trajectories. (c) Fragments of microscopic speeds; bold dashed and dashed-dotted curves $v_{\max}(t)$ and $v_{\min}(t)$ show, respectively, the time-dependence of the maximum and minimum speeds on vehicle trajectories. Vehicle numbers in (c) are the same as those in (a, b). In (a, b), the beginning and end of the on-ramp merging region are, respectively, $x_{\text{on}} = 15$ and $x_{\text{on}}^{(e)} = 15.3$ km.

D. $S \rightarrow F \rightarrow S \rightarrow J$ transitions at bottleneck

Sequences of $S \rightarrow F \rightarrow S \rightarrow J$ transitions found for a homogeneous road (Sec. II F) is also a characteristic effect in synchronized flow at the bottleneck (Figs. 17 and 18) caused by the competition of the $S \rightarrow F$ and $S \rightarrow J$ instabilities.

In a sequence of $S \rightarrow F \rightarrow S \rightarrow J$ transitions at the bottleneck, the first $S \rightarrow F$ transition results from the development of an $S \rightarrow F$ instability (labeled by dashed curves in Fig. 17 (a, c)). A growing wave of the local speed increase caused by the $S \rightarrow F$ instability is initiated by a speed peak that occurs at the bottleneck (labeled by “speed peak” in Fig. 17 (b)). The physics of the speed peak and of the development of the $S \rightarrow F$ instability is

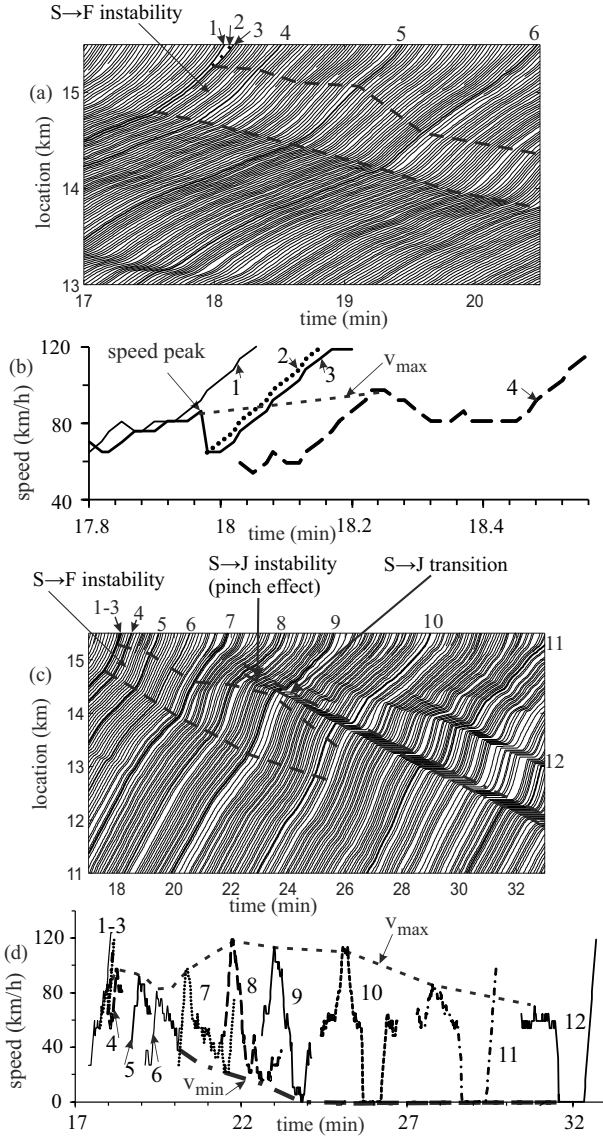


FIG. 17: Continuation of Fig. 12 (e). S→F→S→J transitions at bottleneck: (a, c) Fragments of vehicle trajectories in different scales; in (a) each vehicle trajectory is shown; in (c) each 3rd vehicle trajectory is shown. (b, d) Fragments of microscopic speeds; bold dashed and dashed-dotted curves $v_{\max}(t)$ and $v_{\min}(t)$ show, respectively, the time-dependence of the maximum and minimum speeds on vehicle trajectories; vehicle numbers in (b, d) are the same as those in (a, c). In (a, c), the beginning and end of the on-ramp merging region are, respectively, $x_{\text{on}} = 15$ and $x_{\text{on}}^{(e)} = 15.3$ km.

qualitatively the same as that found already in [43, 121].

The second S→J transition in the sequence of S→F→S→J transitions results from the occurrence of the pinch effect in synchronized flow (labeled by “pinch effect” in Figs. 18 (a, c–e)). The pinch effect is realized downstream of the wave of the local speed increase: During the vehicle deceleration at the downstream front of this wave to a synchronized flow speed (see the speed

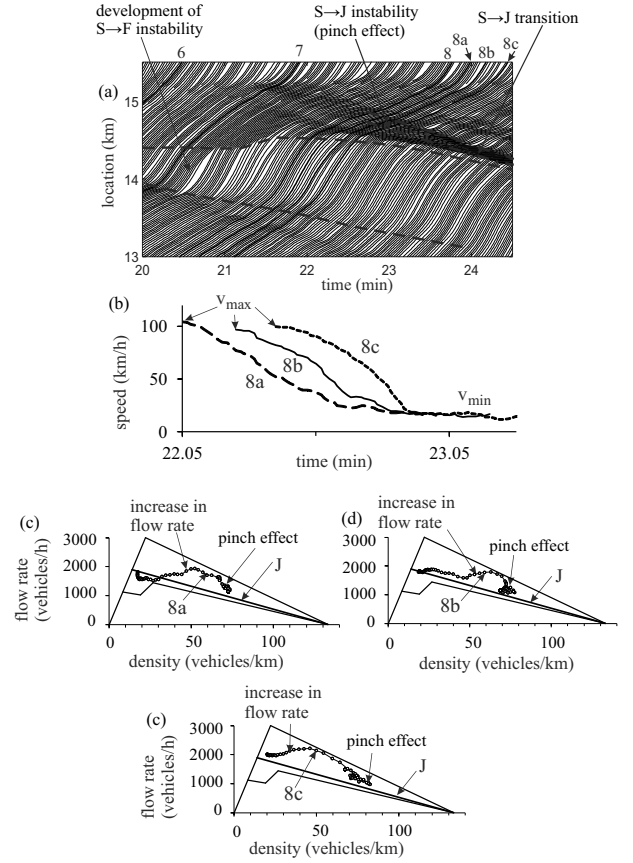


FIG. 18: Continuation of Fig. 17 (c): (a) Fragment of vehicle trajectories; vehicle numbers 6 and 7 are, respectively, the same as those in Fig. 17 (c). (b) Fragments of microscopic speeds. (c–e) Points along vehicle trajectories in the flow–density plane; averaging over 10 vehicles upstream of the related vehicle for each time step (1 sec). Vehicle numbers in (b–e) are the same as those in (a). In (a), the beginning and end of the on-ramp merging region are, respectively, $x_{\text{on}} = 15$ and $x_{\text{on}}^{(e)} = 15.3$ km.

reduction of vehicles 8a, 8b, and 8c in Fig. 18 (b)), the flow rate increases (labeled by “increase in flow rate” in Figs. 18 (c–e)) and then the density in synchronized flow increases strongly (labeled by “pinch effect” in Figs. 18 (c–e)). The pinch effect causes the emergence of a growing narrow moving jam (S→J instability) (labeled by “S→J instability” in Fig. 18 (a)). A growing narrow moving jam resulting from the pinch effect causes an S→J transition (Figs. 17 (c) and 18 (a)).

The above physics of the second S→J transition in the sequence of S→F→S→J transitions at the bottleneck is the same as that on the homogeneous road (Sec. IIF). To explain this, we note that after the growing wave of the local speed increase has occurred in synchronized flow at the bottleneck, the subsequent development of the pinch effect with resulting the S→J instability downstream of the wave is realized far upstream of the bottleneck. Therefore, this second S→J instability in the

sequence of $S \rightarrow F \rightarrow S \rightarrow J$ transitions does not almost depend on the bottleneck existence.

IV. DISCUSSION

A. Effect of initial space gap on phase transitions in synchronized flow on homogeneous road

1. Averaged speed in synchronized flow

It has been found that when the initial space-gap g_{ini} between vehicles has been chosen (for example, $g_{\text{ini}} = 19.5$ m in Fig. 2), neither probabilities P_S , P_{SF} , P_{SJ} (Fig. 3) nor qualitative features of phase transitions and resulting congested patterns (Fig. 2) depend on the value of the initial synchronized flow speed $v_{\text{ini}}^{(\text{syn})}$: Regardless of the choice of the initial synchronized flow speed, during a short time interval (about 1–2 min that can be considered negligible in comparison with the chosen time interval of traffic observation $T_{\text{ob}} = 60$ min) due to a random vehicle acceleration and deceleration the average synchronized flow speed tends to some almost time-independent value $v_{\text{av}}^{(\text{syn})}$ for a given $g_{\text{ini}} = \bar{g}$. This speed is a space-gap function $v_{\text{av}}^{(\text{syn})}(\bar{g})$ (solid curve $v_{\text{av}}^{(\text{syn})}(\bar{g})$ in Fig. 19 (a)).

Obviously that the function $v_{\text{av}}^{(\text{syn})}(\bar{g})$ exists within the space-gap range (2) within which $P_S > 0$. However, it has been found that the function $v_{\text{av}}^{(\text{syn})}(\bar{g})$ can be calculated even when $P_S = 0$ (Fig. 3 (a)), however, only in some short space-gap ranges related to $\bar{g} < g_S$ and to $\bar{g} > g_{\text{max}}$ that are outside range (2). This is because condition $P_S = 0$ means that an $S \rightarrow F$ transition does occur in synchronized flow during the time interval T_{ob} . As above-mentioned, this time interval is considerably longer than a short time interval of the reaching of the average synchronized flow speed $v_{\text{av}}^{(\text{syn})}$. However, if either \bar{g} becomes considerably smaller than g_S or \bar{g} becomes considerably larger than g_{max} , the mean time delay of the $S \rightarrow F$ transition decreases to short enough values at which the average synchronized flow speed $v_{\text{av}}^{(\text{syn})}$ cannot be calculated any more. This explains the existence of boundaries of the space-gap function $v_{\text{av}}^{(\text{syn})}(\bar{g})$ in Fig. 19 (a) as well as of boundaries of the density function $v_{\text{av}}^{(\text{syn})}(\rho)$ in Fig. 19 (b).

2. Phase transitions and resulting congested patterns

As follows from Fig. 3, for space gap $g_{\text{ini}} = 19.5$ m chosen in Fig. 2 probabilities $P_{SF} = 0.425$ and $P_{SJ} = 0.5$ are close each other. The subsequent strong spatiotemporal competition between $S \rightarrow F$ and $S \rightarrow J$ instabilities results in the occurrence of the diverse variety of unknown features of congested traffic patterns as well as effects like se-

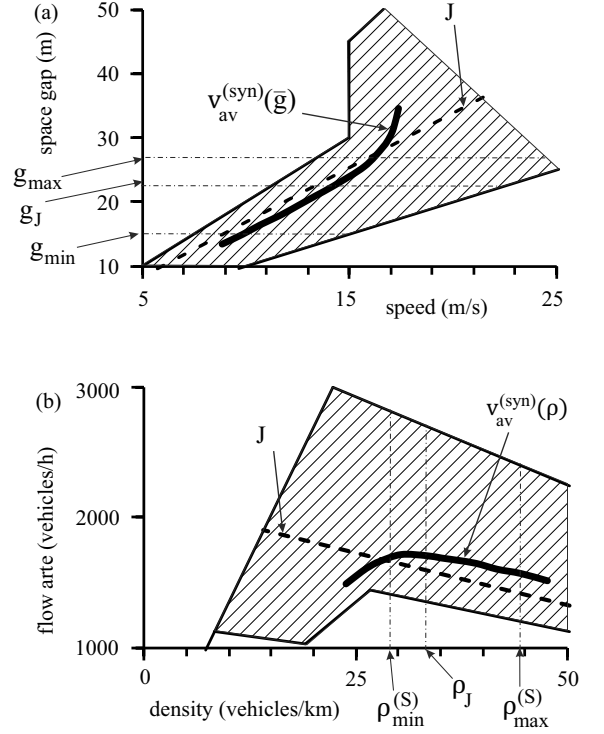


FIG. 19: A part of steady states of synchronized flow in the KKSW CA model (dashed regions) in the space-gap-speed (a) and flow-density (b) planes together with average speed in synchronized flow (respectively, solid curves $v_{\text{av}}^{(\text{syn})}(\bar{g})$ and $v_{\text{av}}^{(\text{syn})}(\rho)$) and with lines J (dashed lines J). $\rho_{\text{max}}^{(S)} = 1000/(d + g_{\text{min}})$, $\rho_J = 1000/(d + g_J)$, $\rho_{\text{min}}^{(S)} = 1000/(d + g_{\text{max}})$ (vehicles/km), d is vehicle length.

quences of $S \rightarrow F \rightarrow S \rightarrow J$ transitions and $S \rightarrow J \rightarrow S \rightarrow F$ transitions studied in Sec. II.

Here we discuss features of congested patterns when the spatiotemporal competition between $S \rightarrow F$ and $S \rightarrow J$ instabilities becomes weaker. This can be expected when due to the change in g_{ini} the difference between probabilities P_{SF} and P_{SJ} becomes larger.

When g_{ini} increases, probability P_{SF} increases, whereas probability P_{SJ} decreases (Fig. 3). Respectively, we have found that an $S \rightarrow F$ instability governs mostly the emergence of the phases F and/or J in an initial synchronized flow (Fig. 20). The larger the chosen average space gap g_{ini} is, the more frequently one or a few moving synchronized flow patterns (MSP) appear spontaneously (some of the MSPs are labeled by “MSP” in Fig. 20). MSPs emergence shown in Fig. 20 (b–d, g, h) is well-known effect [6]. However, it has been unknown that due to the spatiotemporal competition between $S \rightarrow F$ and $S \rightarrow J$ instabilities the initial $S \rightarrow F$ instability while causing a growing wave of a local speed increase in synchronized flow can result in an $S \rightarrow J$ instability downstream of the wave. This effect (Sec. II F) results in $S \rightarrow F \rightarrow S \rightarrow J$ transitions even then, when probability P_{SJ} is very small (Fig. 20 (a)) or $P_{SJ} = 0$ (Fig. 20 (b, c, g)).

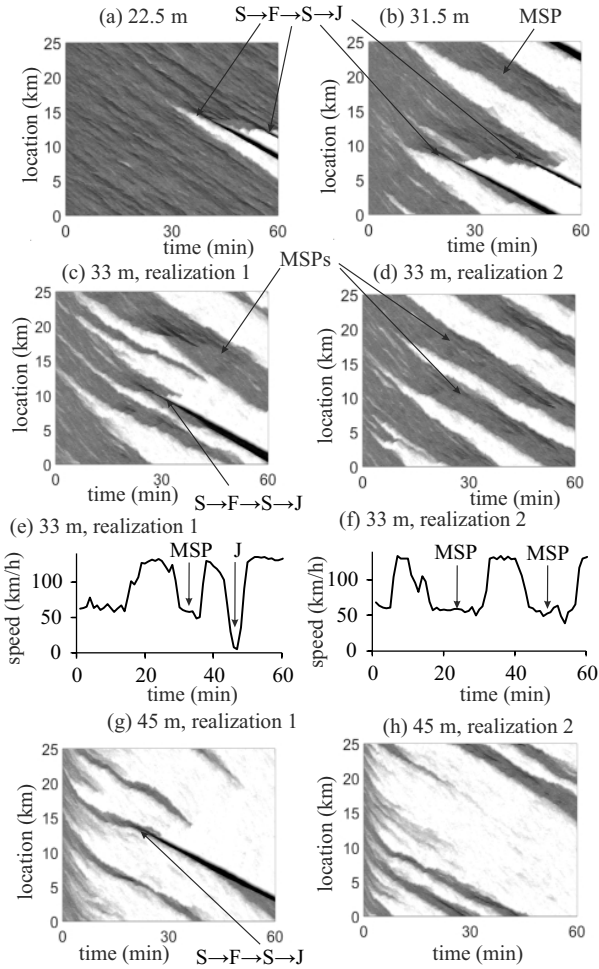


FIG. 20: Effect of the increase in initial average space gap between vehicles on resulting congested patterns on homogeneous road: (a) One of the realizations at $g_{ini} = 22.5$ m, $v_{ini}^{(syn)} = 48.6$ km/h. (b) One of the realizations at $g_{ini} = 31.5$ m, $v_{ini}^{(syn)} = 59.4$ km/h. (c, d) Two realizations at $g_{ini} = 33$ m, $v_{ini}^{(syn)} = 64.8$ km/h. (e, f) Time-dependencies of average speed (1 min averaged data) measured at virtual detectors at $x = 3$ km for (c, d), respectively. (g, h) Two realizations at $g_{ini} = 45$ m, $v_{ini}^{(syn)} = 64.8$ km/h. Other model parameters are the same as those in Fig. 2. In (a–d, g, h), vehicle speed data presented by regions with variable shades of gray (shades of gray vary from white to black when the speed decreases from 120 km/h (white) to 0 km/h (black)). Values $(P_{SF}, P_{SJ}) = (0.65, 0.08)$ (a), $(1.0, 0)$ (b–h). Arrows $S \rightarrow F \rightarrow S \rightarrow J$ label some of the sequences of $S \rightarrow F \rightarrow S \rightarrow J$ transitions. MSP is a moving synchronized flow pattern.

When g_{ini} decreases, probability P_{SF} decreases, whereas probability P_{SJ} increases (Fig. 3). Respectively, we have found that an $S \rightarrow J$ instability governs mostly the emergence of the phases J and/or F in an initial synchronized flow (Fig. 21). The smaller the chosen average space gap g_{ini} is, the more frequently one or a few wide moving jams appear spontaneously (Fig. 21). The wide moving jam emergence is well-known effect [6]. However,

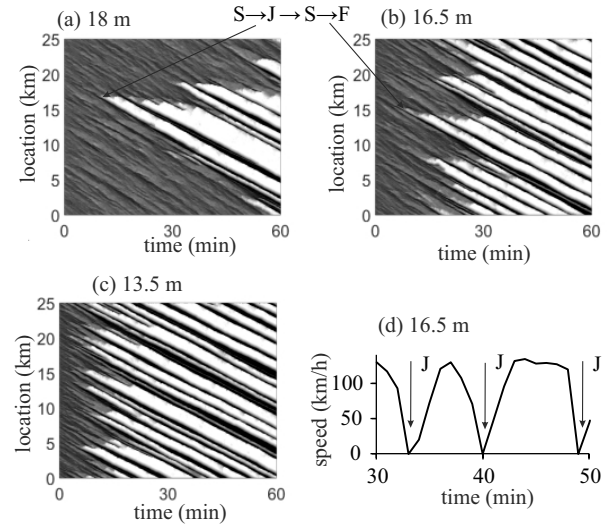


FIG. 21: Effect of the decrease in initial average space gap between vehicles on resulting congested patterns on homogeneous road: (a) One of the realizations at $g_{ini} = 18$ m, $v_{ini}^{(syn)} = 43.2$ km/h. (b) One of the realizations at $g_{ini} = 16.5$ m, $v_{ini}^{(syn)} = 37.8$ km/h. (c) One of the realizations at $g_{ini} = 13.5$ m, $v_{ini}^{(syn)} = 32.4$ km/h. (d) Time-dependence of average speed (1 min averaged data) measured at a virtual detector at $x = 7$ km for (b). Other model parameters are the same as those in Fig. 2. In (a–c), vehicle speed data presented by regions with variable shades of gray (shades of gray vary from white to black when the speed decreases from 120 km/h (white) to 0 km/h (black)). Values $(P_{SF}, P_{SJ}) = (0.2, 0.8)$ (a), $(0.05, 0.95)$ (b), $(0, 1.0)$ (c). Arrows $S \rightarrow J \rightarrow S \rightarrow F$ label some of the sequences of $S \rightarrow J \rightarrow S \rightarrow F$ transitions.

it has been unknown that due to the spatiotemporal competition between $S \rightarrow F$ and $S \rightarrow J$ instabilities the initial $S \rightarrow J$ instability while causing a growing narrow moving jam can result in an $S \rightarrow F$ instability downstream of the moving jam. This effect (Sec. II D) results in $S \rightarrow J \rightarrow S \rightarrow F$ transitions even then, when probability P_{SF} is very small (Fig. 21 (a, b)) or $P_{SF} = 0$ (Fig. 21 (c)).

B. Effect of on-ramp inflow rate on phase transitions in synchronized flow at bottleneck

The effect of the average space gap between vehicles on phase transitions and resulting congested patterns on the homogeneous road (Sec. IV A 2) is qualitatively similar to the effect of the on-ramp inflow rate on phase transitions and resulting congested patterns at the bottleneck (Figs. 22 and 23).

When q_{on} decreases, probability P_{SF} increases, whereas probability P_{SJ} decreases (Fig. 13). Respectively, we have found that an $S \rightarrow F$ instability governs mostly the emergence of the phases F and/or J in synchronized flow at the bottleneck (Fig. 22). As well-known [6], the smaller q_{on} is, the more frequently MSPs appear spon-

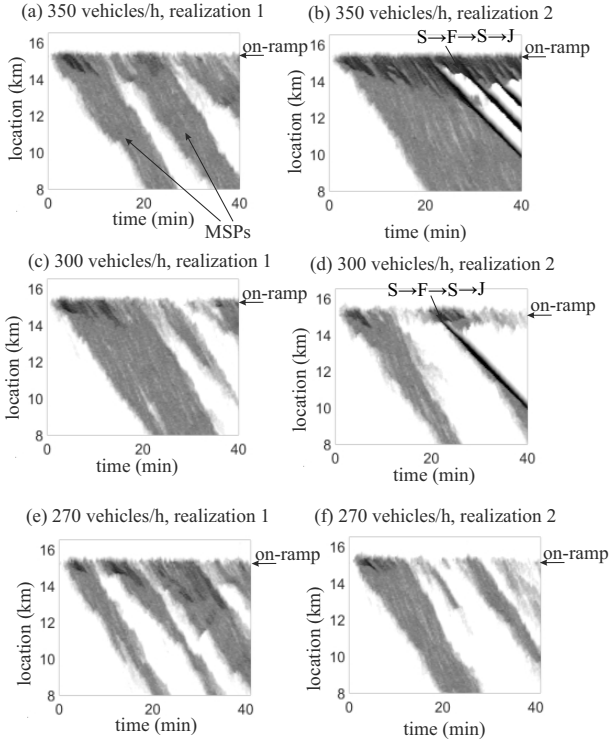


FIG. 22: Effect of the decrease in on-ramp inflow q_{on} on resulting congested patterns at bottleneck at the same other model parameters as those in Fig. 12: (a, b) Two realizations at $q_{on} = 350$ vehicles/h. (c, d) Two realizations at $q_{on} = 300$ vehicles/h. (e, f) Two realizations at $q_{on} = 270$ vehicles/h. In (a–f), vehicle speed data presented by regions with variable shades of gray (shades of gray vary from white to black when the speed decreases from 120 km/h (white) to 0 km/h (black)). Values $(P_{SF}, P_{SJ}) = (0.6, 0.125)$ (a, b), $(1.0, 0)$ (c–f). Arrows $S \rightarrow F \rightarrow S \rightarrow J$ label some of the sequences of $S \rightarrow F \rightarrow S \rightarrow J$ transitions.

taneously (some of the MSPs are labeled by “MSP” in Fig. 22). However, it has been unknown that due to the spatiotemporal competition between $S \rightarrow F$ and $S \rightarrow J$ instabilities the initial $S \rightarrow F$ instability can result in an $S \rightarrow J$ instability upstream of the bottleneck. This effect (Sec. III D) results in $S \rightarrow F \rightarrow S \rightarrow J$ transitions even then, when probability P_{SJ} is very small (Fig. 22 (b)) or $P_{SJ} = 0$ (Fig. 22 (d)).

When q_{on} increases, probability P_{SF} decreases, whereas probability P_{SJ} increases (Fig. 13). Respectively, we have found that an $S \rightarrow J$ instability governs mostly the emergence of the phases J and/or F in an initial synchronized flow at the bottleneck (Fig. 23). As well-known [6], the larger q_{on} is, the more frequently one or a few wide moving jams appear spontaneously (Fig. 23). However, it has been unknown that due to the spatiotemporal competition between $S \rightarrow F$ and $S \rightarrow J$ instabilities the initial $S \rightarrow J$ instability can result in an $S \rightarrow F$ instability upstream of the bottleneck. This effect (Sec. III C) results in $S \rightarrow J \rightarrow S \rightarrow F$ transitions even then, when probability

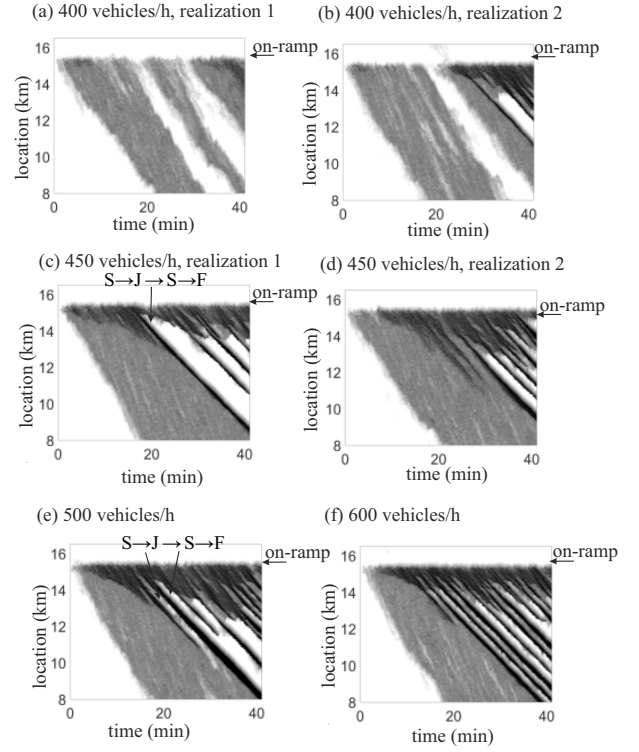


FIG. 23: Effect of the increase in on-ramp inflow q_{on} on resulting congested patterns at bottleneck at the same other model parameters as those in Fig. 12: (a, b) Two realizations at $q_{on} = 400$ vehicles/h. (c, d) Two realizations at $q_{on} = 450$ vehicles/h. (e) One of the realizations at $q_{on} = 500$ vehicles/h. (f) One of the realizations at $q_{on} = 600$ vehicles/h. In (a–f), vehicle speed data presented by regions with variable shades of gray (shades of gray vary from white to black when the speed decreases from 120 km/h (white) to 0 km/h (black)). Values $(P_{SF}, P_{SJ}) = (0.3, 0.65)$ (a, b), $(0.05, 0.95)$ (c, d), $(0, 1.0)$ (e, f). Arrows $S \rightarrow J \rightarrow S \rightarrow F$ label some of the sequences of $S \rightarrow J \rightarrow S \rightarrow F$ transitions.

P_{SF} is very small (Fig. 23 (c, d)) or $P_{SF} = 0$ (Fig. 23 (e, f)).

C. $F \rightarrow S \rightarrow F$ transitions before traffic breakdown and phase transitions in synchronized flow at bottleneck

In the above study of statistical physics of synchronized flow at the bottleneck (Secs. III and IV B), we have induced the synchronized flow through the use of the initial on-ramp inflow impulse. In real traffic, synchronized flow occurs often spontaneously due to a random time-delayed traffic breakdown ($F \rightarrow S$ transition) at the bottleneck. In [43] it has been found that a random time delay $T^{(B)}$ of this $F \rightarrow S$ transition is governed by sequence(s) of $F \rightarrow S \rightarrow F$ transitions that interrupt the development of a congested pattern at the bottleneck: Firstly, an $F \rightarrow S$ transition has occurred at the bottleneck; then, in the

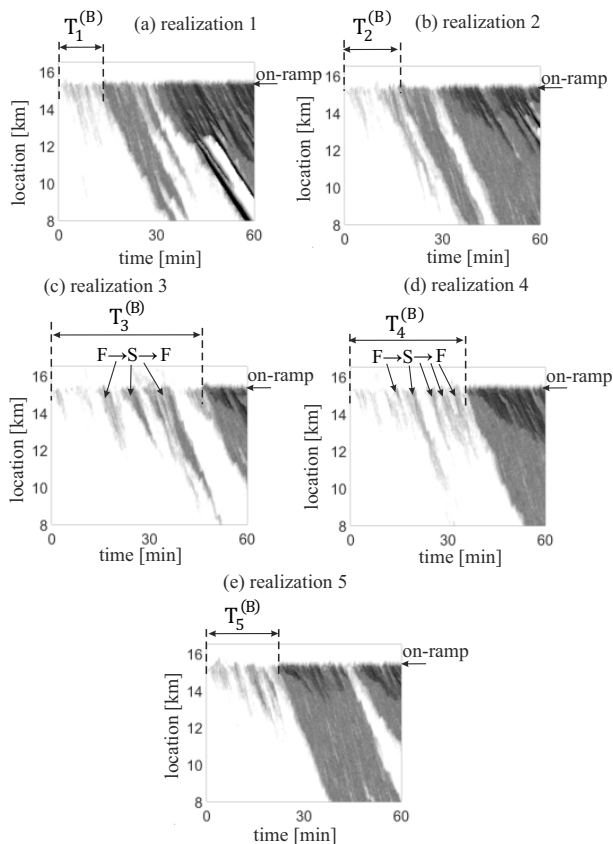


FIG. 24: $F \rightarrow S \rightarrow F$ transitions and phase transitions in synchronized flow at bottleneck: (a–e) five different realizations of spontaneous emergence of synchronized flow at the bottleneck. The flow rates q_{in} , q_{on} and other model parameters are the same as those in Fig. 12. The only one difference is that whereas in Fig. 12 synchronized flow has been induced at the bottleneck, in (a–e) synchronized flow has emerged at the bottleneck spontaneously after a random time delay $T_i^{(B)}$ ($i = 1, 2, \dots, 5$ is the realization number) caused by $F \rightarrow S \rightarrow F$ transitions before traffic breakdown. In (a–e), vehicle speed data presented by regions with variable shades of gray (shades of gray vary from white to black when the speed decreases from 120 km/h (white) to 0 km/h (black)). Arrows $F \rightarrow S \rightarrow F$ label some of the sequences of $F \rightarrow S \rightarrow F$ transitions.

emergent synchronized flow the $S \rightarrow F$ instability is realized that leads to an $S \rightarrow F$ transition; finally, free flow returns at the bottleneck and the emergent synchronized flow dissolves (called as “dissolving synchronized flow” at the bottleneck). Recently, sequences of $F \rightarrow S \rightarrow F$ transitions before traffic breakdown predicted in [43] have indeed been observed in real field traffic data [122]. Thus, a question arises: Do sequences of $F \rightarrow S \rightarrow F$ transitions effect on statistical physical features of synchronized flow found above in this paper?

Simulations show that none of qualitative conclusions about statistical physics of synchronized flow at the bottleneck found above change, when synchronized flow occurs spontaneously at the bottleneck. Some of simulation

realizations for this case made at the same model parameters as those in Fig. 12 are presented in Fig. 24.

D. Conclusions

A spatiotemporal competition between $S \rightarrow F$ and $S \rightarrow J$ instabilities is responsible for the following main statistical features of synchronized flow revealed in the paper:

1. There is a finite range of the initial space-gap between vehicles in synchronized flow within which during a chosen time for traffic observations either synchronized flow persists with probability P_S , or firstly an $S \rightarrow F$ transition occurs in synchronized flow with probability P_{SF} , or else firstly an $S \rightarrow J$ transition occurs in synchronized flow with probability P_{SJ} .

2. An initial $S \rightarrow F$ instability can cause the subsequent $S \rightarrow J$ instability downstream in synchronized flow while leading to the occurrence of a sequence of $S \rightarrow F \rightarrow S \rightarrow J$ transitions.

3. An initial $S \rightarrow J$ instability can cause the subsequent $S \rightarrow F$ instability downstream in synchronized flow while leading to the occurrence of a sequence of $S \rightarrow J \rightarrow S \rightarrow F$ transitions.

4. Each of the phase transitions in sequences of $S \rightarrow F \rightarrow S \rightarrow J$ and $S \rightarrow J \rightarrow S \rightarrow F$ transitions exhibits the nucleation nature. This result determines the spatiotemporal complexity of traffic patterns.

5. At the same model parameters, there can be a large number of qualitatively different simulation realizations in which different sequences of $S \rightarrow F$ and $S \rightarrow J$ instabilities at random road locations are realized. The diverse variety of time-sequences of $S \rightarrow F$ and $S \rightarrow J$ instabilities occurring at random road locations can cause different nucleation-interruption effects as well as different time-sequences of $S \rightarrow F \rightarrow S \rightarrow J$ and $S \rightarrow J \rightarrow S \rightarrow F$ phase transitions.

6. Statistical features of vehicular traffic found for a homogeneous road remain qualitatively for a road with a bottleneck. In particular, flow-rate dependencies of probabilities P_S , P_{SF} , and P_{SJ} at the bottleneck are qualitatively the same as the space-gap dependencies of these probabilities found in the paper for the homogeneous road.

7. The main difference between the homogeneous road and the road with the bottleneck is that due to a permanent non-homogeneity introduced by the bottleneck, nuclei for initial $S \rightarrow F$ and $S \rightarrow J$ instabilities appear mostly at the bottleneck rather than at random locations on the homogeneous road.

8. The phenomena of the $S \rightarrow F \rightarrow S \rightarrow J$ transitions and the $S \rightarrow J \rightarrow S \rightarrow F$ transitions caused by the competition of the $S \rightarrow F$ and $S \rightarrow J$ instabilities, which have been found in the paper both for the homogeneous road and for the road with the bottleneck are common critical phenomena in synchronized flow. These spatiotemporal traffic phenomena explain complex alternations of free flow regions with wide moving jams that occur when either the

S→J instability (Figs. 2 (b, c) and 12 (b, c)) or the S→F instability (Figs. 2 (d, e) and 12 (d, e)) is realized.

9. More complex spatiotemporal traffic phenomena have been found when in the same simulation realization a time-sequence of S→J and S→F instabilities is realized. Examples in which firstly an S→J instability occurs and later an S→F instability is realized are shown for realization 6 for the homogeneous road (Fig. 2 (f)) as well as for realization 6 for the road with the bottleneck (Fig. 12 (f)). Other examples in which firstly an S→F instability occurs and later an S→J instability is realized are shown for realization 7 for the homogeneous road (Fig. 2 (g)) as well as for realization 7 for the road with the bottleneck (Fig. 12 (g)).

Appendix A: KKSJ CA model

In all simulations we have used the KKSJ CA three-phase traffic flow model [45, 56, 57]. The physics of the KKSJ CA model has been considered in details in Appendix B of the book [8]. In the KKSJ CA model for identical drivers and vehicles moving on a single-lane road [57], the following designations for main variables and vehicle parameters are used: $n = 0, 1, 2, \dots$ is the number of time steps; $\tau = 1$ s is time step; $\delta x = 1.5$ m is space step; x_n and v_n are the coordinate and speed of the vehicle; time and space are measured in units of τ and δx , respectively; v_{free} is the maximum speed in free flow; $g_n = x_{\ell, n} - x_n - d$ is a space gap between two vehicles following each other; the lower index ℓ marks variables related to the preceding vehicle; d is vehicle length; G_n is a synchronization space gap.

The KKSJ CA model consists of the following sequence of rules [57]:

- (a) “comparison of vehicle gap with the synchronization gap”:

$$\text{if } g_n \leq G(v_n)$$

then follow rules (b), (c) and skip rule (d), (A1)

$$\text{if } g_n > G(v_n)$$

then skip rules (b), (c) and follow rule (d), (A2)

- (b) “speed adaptation within synchronization gap” is given by formula:

$$v_{n+1} = v_n + \text{sgn}(v_{\ell, n} - v_n), \quad (\text{A3})$$

- (c) “over-acceleration through random acceleration within synchronization gap” is given by formula

if $v_n \geq v_{\ell, n}$, then with probability p_a ,

$$v_{n+1} = \min(v_{n+1} + 1, v_{\text{free}}), \quad (\text{A4})$$

- (d) “acceleration”:

$$v_{n+1} = \min(v_n + 1, v_{\text{free}}), \quad (\text{A5})$$

- (e) “deceleration”:

$$v_{n+1} = \min(v_{n+1}, g_n), \quad (\text{A6})$$

- (f) “randomization” is given by formula:

$$\text{with probability } p, \quad v_{n+1} = \max(v_{n+1} - 1, 0), \quad (\text{A7})$$

- (g) “motion” is described by formula:

$$x_{n+1} = x_n + v_{n+1}. \quad (\text{A8})$$

Formula (A4) is applied, when

$$r < p_a, \quad (\text{A9})$$

formula (A7) is applied, when

$$p_a \leq r < p_a + p, \quad (\text{A10})$$

where $p_a + p \leq 1$; $r = \text{rand}()$ is a random value distributed uniformly between 0 and 1. Probability of over-acceleration p_a in (A4) is chosen as the increasing speed function:

$$p_a(v_n) = p_{a,1} + p_{a,2} \max(0, \min(1, (v_n - v_{\text{syn}})/\Delta v_{\text{syn}})), \quad (\text{A11})$$

where $p_{a,1}$, $p_{a,2}$, v_{syn} and Δv_{syn} are constants. In (A1), (A2),

$$G(v_n) = kv_n. \quad (\text{A12})$$

The rules of vehicle motion (A2)–(A12) (without formula (A11)) have been formulated in the KKW (Kerner-Klenov-Wolf) CA model [45]. In comparison with the KKW CA model [45], we use in (A7), (A10) for probability p formula

$$p = \begin{cases} p_2 & \text{for } v_{n+1} > v_n, \\ p_3 & \text{for } v_{n+1} \leq v_n, \end{cases} \quad (\text{A13})$$

which has been used in the KKSJ CA model of Ref. [56]. The importance of formula (A13) is as follows. This rule of vehicle motion leads to a time delay in vehicle acceleration at the downstream front of synchronized flow. In other words, this is an additional mechanism of time delay in vehicle acceleration in comparison with a well-known slow-to-start rule [123, 124]:

$$p_2(v_n) = \begin{cases} p_0^{(2)} & \text{for } v_n = 0, \\ p_1^{(2)} & \text{for } v_n > 0 \end{cases} \quad (\text{A14})$$

that is also used in the KKSJ CA model. However, in the KKSJ CA model in formula (A14) probability $p_1^{(2)}$ is chosen to provide a delay in vehicle acceleration only if the vehicle does not accelerate at previous time step n :

$$p_1^{(2)} = \begin{cases} p_2^{(2)} & \text{for } v_n \leq v_{n-1}, \\ 0 & \text{for } v_n > v_{n-1}. \end{cases} \quad (\text{A15})$$

In (A13)–(A15), p_3 , $p_0^{(2)}$, and $p_2^{(2)}$ are constants. We also assume that in (A12) [45]

$$k(v_n) = \begin{cases} k_1 & \text{for } v_n > v_{\text{pinch}}, \\ k_2 & \text{for } v_n \leq v_{\text{pinch}}, \end{cases} \quad (\text{A16})$$

where v_{pinch} , k_1 , and k_2 are constants ($k_1 > k_2 \geq 1$).

The rule of vehicle motion (A13) of the KKS model [56] together with formula (A11) allows us to improve characteristics of synchronized flow patterns (SP) simulated with the KKS model (A2)–(A16) for a single-lane road. Other physical features of the KKS

model have been explained in [56].

A model of an on-ramp bottleneck that has been used for simulations of single-lane road with the on-ramp bottleneck as well as parameters of the model are the same as those presented in Appendix B of the book [8].

Acknowledgments: We thank our partners for their support in the project “MEC-View – Object detection for automated driving based on Mobile Edge Computing”, funded by the German Federal Ministry of Economic Affairs and Energy. I thank Sergey Klenov for discussions and help in simulations.

-
- [1] L.C. Edie, *Oper. Res.* **2** 107–138 (1954); L.C. Edie, *Oper. Res.* **9** 66–77 (1961); L.C. Edie, E. Baverez, in *Third Int. Sym. on the Theory of Traffic Flow*, 1995, pp. 26–37; L.C. Edie, R.S. Foote, in *Highway Research Board Proceedings*, (HRB, National Research Council, Washington, D.C., 1958), **37**, pp. 334–344; L.C. Edie, R.S. Foote, in *Highway Research Board Proceedings*, (HRB, National Research Council, Washington, D.C., 1960), **39**, pp. 492–505
- [2] M. Koshi, M. Iwasaki, I. Ohkura, in *Proc. 8th International Symposium on Transportation and Traffic Theory*, edited by V.F. Hurdle. (University of Toronto Press, Toronto, Ontario, 1983), pp. 403
- [3] J. Treiterer, *Transportation Research* **1** 231–251 (1967); J. Treiterer, “Investigation of Traffic Dynamics by Aerial Photogrammetry Techniques”, *Ohio State University Technical Report PB 246 094*, (Columbus, Ohio, 1975); J. Treiterer, J.A. Myers, in *Procs. 6th International Symposium on Transportation and Traffic Theory*, ed. by D.J. Buckley. (A.H. & AW Reed, London, 1974), pp. 13–38; J. Treiterer, J.I. Taylor, *Highway Res. Rec.* **142** 1–12 (1966)
- [4] B.S. Kerner, *Phys. Rev. Lett.* **81**, 3797–3400 (1998).
- [5] B.S. Kerner, *Trans. Res. Rec.* **1678**, 160–167 (1999); B.S. Kerner, in *Transportation and Traffic Theory*, ed. by A. Ceder. (Elsevier Science, Amsterdam 1999), pp. 147–171; B.S. Kerner, *Physics World* **12**, 25–30 (August 1999).
- [6] B.S. Kerner. *The Physics of Traffic* (Springer, Berlin, New York 2004)
- [7] B.S. Kerner. *Introduction to Modern Traffic Flow Theory and Control*. (Springer, Berlin, New York, 2009).
- [8] B.S. Kerner. *Breakdown in Traffic Networks*. (Springer, Berlin, New York, 2017).
- [9] B.S. Kerner, H. Rehborn, R.-P. Schäfer, S. L. Klenov, J. Palmer, S. Lorkowski, N. Witte, *Physica A* **392** 221–251 (2013).
- [10] R. Herman, E.W. Montroll, R.B. Potts, R.W. Rothery, *Oper. Res.* **7** 86–106 (1959).
- [11] D.C. Gazis, R. Herman, R.B. Potts, *Oper. Res.* **7** 499–505 (1959).
- [12] D.C. Gazis, R. Herman, R.W. Rothery, *Oper. Res.* **9** 545–567 (1961).
- [13] R.E. Chandler, R. Herman, E.W. Montroll, *Oper. Res.* **6** 165–184 (1958).
- [14] G.F. Newell, *Oper. Res.* **9**, 209–229 (1961).
- [15] G.F. Newell, ‘Instability in dense highway traffic, a review’. In: *Proc. Second Internat. Sympos. on Traffic Road Traffic Flow* (OECD, London 1963) pp. 73–83.
- [16] G.F. Newell, *Transp. Res. B* **36**, 195–205 (2002).
- [17] J.A. Laval, C.S. Toth, Y. Zhou, *Transp. Res. B* **70**, 228–238 (2014).
- [18] H.J. Payne, in *Mathematical Models of Public Systems*, ed. by G.A. Bekey. Vol. 1, (Simulation Council, La Jolla, 1971).
- [19] H.J. Payne, *Trans. Res. Rec.* **772**, 68 (1979).
- [20] P.G. Gipps, *Transp. Res. B* **15**, 105–111 (1981).
- [21] P.G. Gipps, *Trans. Res. B.* **20**, 403–414 (1986).
- [22] R. Wiedemann, *Simulation des Verkehrsflusses*, University of Karlsruhe, Karlsruhe, 1974.
- [23] G.B. Whitham, *Proc. R. Soc. London A* **428**, 49 (1990).
- [24] K. Nagel, M. Schreckenberg, *J. Phys. (France) I* **2** 2221–2229 (1992).
- [25] M. Bando, K. Hasebe, A. Nakayama, A. Shibata, Y. Sugiyama, *Phys. Rev. E* **51** 1035–1042 (1995).
- [26] S. Krauß, P. Wagner, C. Gawron, *Phys. Rev. E* **55**, 5597–5602 (1997).
- [27] T. Nagatani, *Physica A* **261**, 599–607 (1998).
- [28] T. Nagatani, *Phys. Rev. E* **59**, 4857–4864 (1999).
- [29] M. Treiber, A. Hennecke, D. Helbing, *Phys. Rev. E* **62**, 1805–1824 (2000).
- [30] A. Aw, M. Rascle, *SIAM J. Appl. Math.* **60**, 916–938 (2000).
- [31] R. Jiang, Q.S. Wu, Z.J. Zhu, *Phys. Rev. E* **64** 017101 (2001).
- [32] A.D. May, *Traffic Flow Fundamentals* (Prentice-Hall, Inc., New Jersey 1990); N.H. Gartner, C.J. Messer, A. Rathi (eds.), *Traffic Flow Theory*, Transportation Research Board, Washington, D.C., 2001; D.C. Gazis, *Traffic Theory*, Springer, Berlin 2002; L. Elefteriadou, *An Introduction to Traffic Flow Theory*, in: *Springer Optimization and its Applications*, vol. 84, Springer, Berlin, 2014.
- [33] D. Helbing, *Rev. Mod. Phys.* **73** 1067–1141 (2001); D. Chowdhury, L. Santen, A. Schadschneider, *Phys. Rep.* **329** 199 (2000); T. Nagatani, *Rep. Prog. Phys.* **65** 1331–1386 (2002); K. Nagel, P. Wagner, R. Woesler, *Oper. Res.* **51** 681–716 (2003); M. Treiber, A. Kesting, *Traffic Flow Dynamics* (Springer, Berlin, 2013).
- [34] B.S. Kerner, *Physica A* **392** 5261–5282 (2013).
- [35] B.S. Kerner, P. Konhäuser *Phys. Rev. E* **48** 2335–2338 (1993); B.S. Kerner, P. Konhäuser *Phys. Rev. E* **50** 54–

- 83 (1994); B.S. Kerner, P. Konhäuser, M. Schilke, Phys. Rev. E **51** 6243–6246 (1995).
- [36] B. S. Kerner, H. Rehborn. Phys. Rev. Lett. **79**, 4030–4033 (1997).
- [37] B.S. Kerner, in *Proceedings of the 3rd Symposium on Highway Capacity and Level of Service*, ed. by R. Rysgaard. Vol 2 (Road Directorate, Ministry of Transport – Denmark, 1998), pp. 621–642; B.S. Kerner, in *Traffic and Granular Flow'97*, ed. by M. Schreckenberg, D.E. Wolf. (Springer, Singapore, 1998), pp. 239–267.
- [38] B.S. Kerner, J. Phys. A: Math. Gen. **33** L221–L228 (2000); B.S. Kerner, in: D. Helbing, H.J. Herrmann, M. Schreckenberg, D.E. Wolf (Eds.), *Traffic and Granular Flow'99: Social, Traffic and Granular Dynamics*, Springer, Heidelberg, Berlin, 2000, pp. 253–284.
- [39] B.S. Kerner, Netw. Spat. Econ. **1**, 35–76 (2001); B.S. Kerner, Transp. Res. Rec. **1802**, 145–154 (2002); B.S. Kerner, in: M.A.P. Taylor (Ed.), *Traffic and Transportation Theory in the 21st Century*, Elsevier Science, Amsterdam, 2002, pp. 417–439; B.S. Kerner, Math. Comput. Modelling **35** 481–508 (2002); B.S. Kerner, in: M. Schreckenberg, Y. Sugiyama, D. Wolf (Eds.), *Traffic and Granular Flow'01*, Springer, Berlin, 2003, pp. 13–50; B.S. Kerner, Physica A **333** 379–440 (2004).
- [40] B.S. Kerner, Phys. Rev. E. **65** 046138 (2002).
- [41] B.S. Kerner, M. Koller, S.L. Klenov, H. Rehborn, M. Leibel, Physica A **438** 365–397 (2015).
- [42] B.S. Kerner, e & i Elektrotechnik und Informationstechnik, **132** 417–433 (2015).
- [43] B.S. Kerner, Phys. Rev. E **92** 062827 (2015).
- [44] B.S. Kerner, S.L. Klenov, J. Phys. A: Math. Gen. **35**, L31–L43 (2002).
- [45] B.S. Kerner, S.L. Klenov, D.E. Wolf, J. Phys. A: Math. Gen. **35**, 9971–10013 (2002).
- [46] B.S. Kerner, S.L. Klenov, Phys. Rev. E **68** 036130 (2003).
- [47] B.S. Kerner, Traffic Breakdown, Modeling Approaches to. In: *Encyclopedia of Complexity and System Science*, ed. by R.A. Meyers. (Springer, Berlin, 2018), https://doi.org/10.1007/978-3-642-27737-5_559-2.
- [48] B.S. Kerner, Traffic Congestion, Spatiotemporal Features of. In: *Encyclopedia of Complexity and System Science*, ed. by R.A. Meyers. (Springer, Berlin, 2018), https://doi.org/10.1007/978-3-642-27737-5_560-2.
- [49] B.S. Kerner, S.L. Klenov, in: *Encyclopedia of Complexity and System Science*, ed. by R.A. Meyers. (Springer, Berlin, 2009), pp. 9282–9302.
- [50] B.S. Kerner, in: *Transportation Research Trends*, ed. by P.O. Inweldi. (Nova Science Publishers, Inc., New York, USA, 2008), pp. 1–92.
- [51] B.S. Kerner, S.L. Klenov, Phys. Rev. E **80** 056101 (2009).
- [52] B.S. Kerner, Physica A **397** 76–110 (2014).
- [53] B.S. Kerner, S.L. Klenov. J. Phys. A: Math. Gen. **37** 8753–8788 (2004).
- [54] B.S. Kerner, J. Phys. A: Math. Theor. **41** 215101 (2008).
- [55] B.S. Kerner, Phys. Rev. E **85** 036110 (2012).
- [56] B.S. Kerner, S.L. Klenov, G. Hermanns, M. Schreckenberg, Physica A, **392** 4083–4105 (2013).
- [57] B.S. Kerner, S.L. Klenov, M. Schreckenberg, Phys. Rev. E, **89**, 052807 (2014).
- [58] B.S. Kerner, S.L. Klenov, M. Schreckenberg, Phys. Rev. E **84** 046110 (2011).
- [59] B.S. Kerner, S.L. Klenov, J. Phys. A: Math. Gen. **39** 1775–1809 (2006).
- [60] B.S. Kerner, Europhys. Lett. **102** 28010 (2013).
- [61] B.S. Kerner, Physica A, **355**, 565–601 (2005); B.S. Kerner, in: *Traffic and Transportation Theory*, edited by H. Mahmassani (Elsevier Science, Amsterdam, 2005), pp. 181–203; B.S. Kerner, S.L. Klenov, A. Hiller. J. Phys. A: Math. Gen. **39**, 2001–2020 (2006); B.S. Kerner, S.L. Klenov, A. Hiller, H. Rehborn. Phys. Rev. E, **73**, 046107 (2006); B.S. Kerner, S.L. Klenov, A. Hiller, Non. Dyn. **49**, 525–553 (2007); B.S. Kerner. IEEE Trans. ITS, **8**, 308–320 (2007); B.S. Kerner, Transp. Res. Rec. **1999**, 30–39 (2007); B.S. Kerner, Transp. Res. Rec. **2088**, 80–89 (2008); B.S. Kerner, S.L. Klenov, Transp. Res. Rec. **2124**, 67–77 (2009); B.S. Kerner, S.L. Klenov, J. Phys. A: Math. Theor. **43**, 425101 (2010); B.S. Kerner, J. Phys. A: Math. Theor. **44** 092001 (2011); B.S. Kerner, Transp. Res. Circular **E-C149**, 22–44 (2011).
- [62] L.C. Davis, Phys. Rev. E **69** 016108 (2004).
- [63] H.K. Lee, R. Barlović, M. Schreckenberg, D. Kim, Phys. Rev. Lett. **92** 238702 (2004).
- [64] R. Jiang, Q.-S. Wu, J. Phys. A: Math. Gen. **37** 8197–8213 (2004).
- [65] K. Gao, R. Jiang, S.-X. Hu, B.-H. Wang, Q.-S. Wu, Phys. Rev. E **76** 026105 (2007).
- [66] L.C. Davis, Physica A **368** 541–550 (2006).
- [67] L.C. Davis, Physica A **361** 606–618 (2006).
- [68] L.C. Davis, Physica A **387** 6395–6410 (2008).
- [69] L.C. Davis, Physica A **388** 4459–4474 (2009).
- [70] L.C. Davis, Physica A **389** 3588–3599 (2010).
- [71] L.C. Davis, Physica A **391** 1679 (2012).
- [72] R. Jiang, M.-B. Hua, R. Wang, Q.-S. Wu, Phys. Lett. A **365** 6–9 (2007).
- [73] R. Jiang, Q.-S. Wu, Phys. Rev. E **72** 067103 (2005).
- [74] R. Jiang, Q.-S. Wu, Physica A **377** 633–640 (2007).
- [75] R. Wang, R. Jiang, Q.-S. Wu, M. Liu, Physica A **378** 475–484 (2007).
- [76] A. Pottmeier, C. Thiemann, A. Schadschneider, M. Schreckenberg, in: A. Schadschneider, T. Pöschel, R. Kühne, M. Schreckenberg, D.E. Wolf (Eds.), *Traffic and Granular Flow'05*, Springer, Berlin, 2007, pp. 503–508.
- [77] X.G. Li, Z.Y. Gao, K.P. Li, X.M. Zhao, Phys. Rev. E **76** 016110 (2007).
- [78] J.J. Wu, H.J. Sun, Z.Y. Gao, Phys. Rev. E **78** 036103 (2008).
- [79] J.A. Laval, in: A. Schadschneider, T. Pöschel, R. Kühne, M. Schreckenberg, D.E. Wolf (Eds.), *Traffic and Granular Flow'05*, Springer, Berlin, 2007, pp. 521–526.
- [80] S. Hoogendoorn, H. van Lint, V.L. Knoop, Trans. Res. Rec. **2088** 102–108 (2008).
- [81] K. Gao, R. Jiang, B.-H. Wang, Q.-S. Wu, Physica A **388** 3233–3243 (2009).
- [82] B. Jia, X.-G. Li, T. Chen, R. Jiang, Z.-Y. Gao, Transportmetrica **7** 127 (2011).
- [83] J.-F. Tian, B. Jia, X.-G. Li, R. Jiang, X.-M. Zhao, Z.-Y. Gao, Physica A **388** 4827–4837 (2009).
- [84] S. He, W. Guan, L. Song, Physica A **389** 825–836 (2009).
- [85] C.-J. Jin, W. Wang, R. Jiang, K. Gao, J. Stat. Mech. P03018 (2010).
- [86] S.L. Klenov, in: V.V. Kozlov (Ed.), *Proc. of Moscow Inst. of Phys. and Technology (Moscow Inst. of Phys. and Technology, Moscow)*, Vol. 2, N. 4 pp. 75–90 (2010) (in Russian).

- [87] A.V. Gasnikov, S.L. Klenov, E.A. Nurminski, Y.A. Kholodov, N.B. Shamray, Introduction to mathematical simulations of traffic flow (MCNMO, Moscow, 2013) (in Russian).
- [88] S. Kokubo, J. Tanimoto, A. Hagishima, *Physica A* **390** 561–568 (2011).
- [89] H.-K. Lee, B.-J. Kim, *Physica A* **390** 4555–4561 (2011).
- [90] C.-J. Jin, W. Wang, *Physica A* **390** 4184–4191 (2011).
- [91] J.P.L. Neto, M.L. Lyra, C.R. da Silva, *Physica A* **390** 3558–3565 (2011).
- [92] P. Zhang, C.-X. Wu, S.C. Wong, *Physica A* **391** 456–463 (2012).
- [93] W.-H. Lee, S.-S. Tseng, J.-L. Shieh, H.-H. Chen, *IEEE Trans. on ITS* **12** 1047–1056 (2011).
- [94] S. Lee, B. Heydecker, Y.H. Kim, E.-Y. Shon, *J. of Adv. Trans.* **45** 143–158 (2011).
- [95] J.-F. Tian, Z.-Z. Yuan, M. Treiber, B. Jia, W.-Y. Zhanga, *Physica A* **391** 3129 (2012).
- [96] R. Borsche, M. Kimathi, A. Klar, *Comp. and Math. with Appl.* **64** 2939–2953 (2012).
- [97] Y. Wang, Y.I. Zhang, J. Hu, L. Li, *Int. J. of Mod. Phys. C* **23** 1250060 (2012).
- [98] J.-F. Tian, Z.-Z. Yuan, B. Jia, H.-q. Fan, T. Wang, *Phys. Lett. A* **376** 2781–2787 (2012).
- [99] Y. Qiu, *J. of Non-Newtonian Fluid Mechanics* **197** 1–4 (2013).
- [100] H. Yang, J. Lu, X. Hu, J. Jiang, *Physica A* **392** 4009 (2013).
- [101] F. Knorr, M. Schreckenberg, *J. Stat. Mech.* P07002 (2013).
- [102] Xiang Zheng-Tao, Li Yu-Jin, Chen Yu-Feng, Xiong Li, *Physica A* **392** 5399 (2013).
- [103] A.R. Mendez, R.M. Velasco, *J. Phys. A: Math. Theor.* **46** 462001 (2013).
- [104] R. Jiang, M.-B. Hu, H.M. Zhang, Z.-Y. Gao, B. Jia, Q.-S. Wu, B. Wang, M. Yang, *PLOS One* **9** e94351 (2014).
- [105] K. Hausken, H. Rehborn, *Game Theoretic Analysis of Congestion, Safety and Security*, in: Springer Series in Reliability Engineering, Springer, Berlin, 2015, pp. 113–141.
- [106] J.F. Tian, M. Treiber, B. Jia, S.F. Ma, B. Jia, W.Y. Zhang, *Transp. Res. B*, **71**, 138–157 (2015).
- [107] R. Jiang, M.B. Hu, H.M. Zhang, Z.Y. Gao, B. Jia, Q.S. Wu, *Transp. Res. B* **80** 338–354 (2015).
- [108] C.-J. Jin, W. Wang, R. Jiang, H.M. Zhang, H. Wang, M.-B. Hud, *Transp. Res. C* **60** 324–338 (2015).
- [109] Ch. Xu, P. Liu, W. Wang, Zh. Li, *Accident Analysis & Prevention* **85**, 45–57 (2015).
- [110] L.C. Davis, *Physica A* **451** 320–332 (2016).
- [111] Y.-S. Qian, X. Feng, J.-W. Zeng, *Physica A* **479** 509–526 (2017)
- [112] J-f Tian, C. Zhu, R Jiang, *Cellular Automaton Models in the Framework of Three-Phase Traffic Theory*. In: Springer Science+Business Media LLC 2018 R. A. Meyers (ed.), *Encyclopedia of Complexity and Systems Science*, https://doi.org/10.1007/978-3-642-27737-5_670-1
- [113] H. Yang, X. Zhai, C. Zheng, *Physica A* **509** 567–577 (2018)
- [114] In [43], it has been found that an S→F instability exhibits the nucleation nature: The S→F instability can occur only, if the amplitude of an initial local speed increase in synchronized flow (called “speed peak”) is large enough. The same nucleation nature of the S→F instability has been found in the case under consideration, when due to an increase in time delay in vehicle acceleration from a moving jam a speed peak appears in synchronized flow downstream of the moving jam: All speed peaks that amplitudes are small enough decay; only when the amplitude of a speed peak exceeds some critical amplitude, an S→F instability is realized.
- [115] The only one difference in simulations of these realizations (Figs. 2 and 12) is a different choice of the initial value (at $t = 0$) of random function *rand()* in the KKS model CA model (see formulas (A9) and (A10) in Appendix A).
- [116] To find the probabilities of the S→F and S→J transitions in an initial synchronized flow, only the most earlier occurring either the S→F transition or the S→J transition has been taken into account.
- [117] Each of the waves of a lower synchronized flow speed (larger density) propagating upstream in synchronized flow (Fig. 14 (a–c)) can also be considered a moving synchronized flow pattern (MSP) surrounded by synchronized flow of a higher synchronized flow speed (smaller density). Because all MSPs in Fig. 14 (a) dissolve over time, the MSPs can be considered dissolving MSPs. Dissolving MSPs have been found both in simulations [52] and in real field traffic data [118] of city traffic upstream of traffic signal.
- [118] S. Kaufmann, B.S. Kerner, H. Rehborn, M. Koller, S.L. Klenov, *Transportation Research C*, **86**, 393–406 (2018).
- [119] It should be noted that the growth of the maximum speed $v_{\max}(t)$ within a speed wave of a local speed increase in synchronized flow on a homogeneous road and also at the bottleneck occurs in a concave way during the development of an S→F instability (Figs. 8 (c) and 16 (c)). Moreover, it turns out that the derivation of this concave growth of the time-function $v_{\max}(t)$ depends on the amplitude of the initial speed disturbance of the local speed increase in synchronized flow. For example, in Fig. 16 (c) the local speed increase on trajectory 5 is considerably smaller than that on trajectory 9. This can explain why the derivation of this concave growth of the time-function $v_{\max}(t)$ between trajectories 5–8 is considerably smaller than that between trajectories 9–12 in Fig. 16 (c). It should be noted that the concave growth of narrow moving jams during the development of an S→J instability has already been known from experimental studies and simulations of moving jam emergence in synchronized flow [104, 107, 120]. As shown in [48], the concave growth of narrow moving jams occurs when the amplitude of the initial disturbance of a local speed decrease initiating the S→J instability is large enough. Thus, we can assume the following general conclusion for both S→F and S→J instabilities: The concave growth of speed waves of either the local speed increase (S→F instability) or decrease (S→J instability) in synchronized flow is realized when the amplitude, respectively, of either the initial local speed increase or initial local speed decrease in synchronized flow is large enough.
- [120] R. Jiang, C.-J. Jin, H.M. Zhang, Y.-X. Huang, J.-F. Tian, W. Wang, M.-B. Hu, H. Wang, B. Jia, *Transportation Research C* **94**, 83–98 (2018).
- [121] We have found a considerably more complex dynamic behavior of the wave of a local speed increase resulting from the S→F instability, in comparison with results of

the development of the S→F instability found in [43]. In particular, the time-function of the wave amplitude $v_{\max}(t)$ firstly increases (dashed curve $v_{\max}(t)$ between trajectories 3 and 4 in Fig. 17 (b)), then it even decreases over time ($v_{\max}(t)$ between trajectories 4–6 in Fig. 17 (b)), later the amplitude begins to increase once more ($v_{\max}(t)$ between trajectories 6–8 in Fig. 17 (c, d)). Finally, the wave amplitude $v_{\max}(t)$ begins to decrease leading to the return F→S transition (dashed curve $v_{\max}(t)$ between trajectories 8–12 in Fig. 17 (d)). There are many other complex cases of the time behavior of the function $v_{\max}(t)$ in which no return F→S transition is realized (see an S→F instability with the

resulting S→F transition in Fig. 12 (d); this case is similar to those cases found in [43]; for this reason, we do not discuss such cases in this paper).

- [122] Sven-Eric Molzahn, Boris S. Kerner, Hubert Rehborn, Sergey L. Klenov, Micha Koller, IET Intelligent Transport Systems **11** 604–612 (2017).
- [123] R. Barlović, L. Santen, A. Schadschneider, M. Schreckenberg, Eur. Phys. J. B **5** 793–800 (1998).
- [124] A. Schadschneider, D. Chowdhury, K. Nishinari, Stochastic Transport in Complex Systems (Elsevier Science Inc., New York, 2011).